Received: 28 November 2020 | Accepted: 9 December 2020

DOI: 10.1002/ppp.2100

RESEARCH ARTICLE

WILEY

Ground-penetrating radar, electromagnetic induction, terrain, and vegetation observations coupled with machine learning to map permafrost distribution at Twelvemile Lake, Alaska

Seth William Campbell[1,2,3] | Martin Briggs[4] | Samuel G. Roy[1,5] | Thomas A. Douglas[6] | Stephanie Saari[6]

[1]University of Maine, School of Earth and Climate Sciences, Orono, Maine, USA

[2]University of Maine, Climate Change Institute, Orono, Maine, USA

[3]U.S. Army Cold Regions Research and Engineering Laboratory, Hanover, New Hampshire, USA

[4]U.S. Geological Survey, Earth System Processes Division, Hydrogeophysics Branch, Storrs, Conneticut, USA

[5]University of Maine, Senator George J. Mitchell Center for Sustainability Solutions, Orono, Maine, USA

[6]U.S. Army Cold Regions Research and Engineering Laboratory, Fort Wainwright, Alaska, USA

Correspondence
Seth Campbell, University of Maine, School of Earth and Climate Sciences, Orono, ME, USA.
Email: scampb64@maine.edu

Funding information
National Science Foundation; Strategic Environmental Research and Development Program

Abstract

We collected ground-penetrating radar (GPR) and frequency-domain electromagnetic induction (FDEM) profiles in 2011 and 2012 to identify the extent of permafrost relative to surface biomass and solar insolation around Twelvemile Lake near Fort Yukon, Alaska. We compared a Landsat-derived biomass estimate and modeled solar insolation from a digital elevation model to the geophysical measurements. We show correspondence between vegetation type and biomass relative to permafrost extent and seasonal freeze–thaw. Thicker permafrost (≥25 m) was covered by greater biomass, and seasonal thaw depths in these regions were minimal (1 m). Shallow (1–3 m depth) and thin (20–50 cm) newly forming permafrost or frozen layers from the previous winter occurred below northward oriented slopes with thin biomass cover. South-facing slopes exhibited permafrost when there was enough biomass to shield incoming solar energy. We developed an artificial neural network to predict permafrost extent across the broader region by mapping GPR-observed instances of permafrost to FDEM, biomass, and terrain observations with 90.2% accuracy. We identified a strong linear correlation (r = −0.77) between permafrost probability and seasonal thaw depth, indicating that our models may also be used to explore thaw patterns and variability in active layer thickness. This study highlights the combined influence of biomass and terrain on the presence of permafrost and the value of evaluating such parameters via remote sensing to predict permafrost spatial or temporal variability. Incorporating diverse geophysical datasets with in-situ validation into machine learning models demonstrates a useful approach to upscale estimated permafrost extent across large Arctic expanses.

KEYWORDS
frequency-domain electromagnetic induction, ground-penetrating radar, machine learning, permafrost, terrain, vegetation

1 | INTRODUCTION

Permafrost underlies ~25% of the land area in the northern hemisphere.[1] An estimated 17% of this area exists as discontinuous permafrost defined as 50%–90% of the land area being influenced by permafrost.[2–4] Central and western Alaska, bound by the Alaska Range to the south and the Brooks Range to the north, consists primarily of discontinuous permafrost generally found underlying valley

bottoms, on north-facing slopes, and in locations where moist, organic-rich soils or snow cover provide thermal stability to preserve year-round frozen ground[3,5–7] (Figure 1). Ecosystem or biomass-protection of permafrost can preserve or allow the aggradation of permafrost over time, even in areas where long-term atmospheric warming is occuring.[8] In permafrost terrains, the active layer undergoes seasonal freezing and thawing whereas the material below the active layer remains frozen year-round. In Alaska, late summer active layer thicknesses range from ~0.1 to 2.2 m and thaw depth is dependent on surface vegetation, biomass, soil type, moisture content, terrain, and local climatology.[9–15] Studies from 1992 to 2016 suggest active layer thickening has occurred across the Arctic, commensurate with increases in Arctic air temperatures.[16]

Concern regarding degradation of permafrost in a warming climate is accentuated due to the potential for significant methane and carbon dioxide release from previously frozen ground and impacts on infrastructure stability.[17,18] Current worldwide estimates of greenhouse gas storage in permafrost are roughly 1,500 Gt.[19] Uncertainties in this pool, and in the fate of this currently frozen carbon when permafrost thaws, is due, in part, to our lack of understanding of permafrost extent, mainly within discontinuous, mountainous, and high plateau regions.[20] Thawing permafrost can influence the surrounding environment through other mechanisms. For example, recently thawed ground can be associated with increased slumping or solifluction,[21] erosion, and sedimentation rates within drainages.[22] These geomorphological processes influence vegetation stability,[23] flora and fauna within watersheds, and, from a societal perspective, geotechnical engineering such as roads, oil pipelines, or vertical infrastructures.[24] Permafrost can also influence near-surface water drainage and shallow groundwater hydrology,[25] both of which impact recharge rates to downstream watersheds. For example, previous results from one of the sites discussed in this paper suggest that re-establishment of permafrost influences groundwater flow and has altered water table levels.[26–28]

Links exist between permafrost distribution and latitude, climate, vegetation, surface slope, aspect, hydrology, geology, snow cover, and forest fire activity. Each variable can influence permafrost across different spatial and temporal scales. For example, thick winter snow cover can act as an insulator from low winter temperatures by not allowing the active layer to refreeze after summer. In contrast, a thin

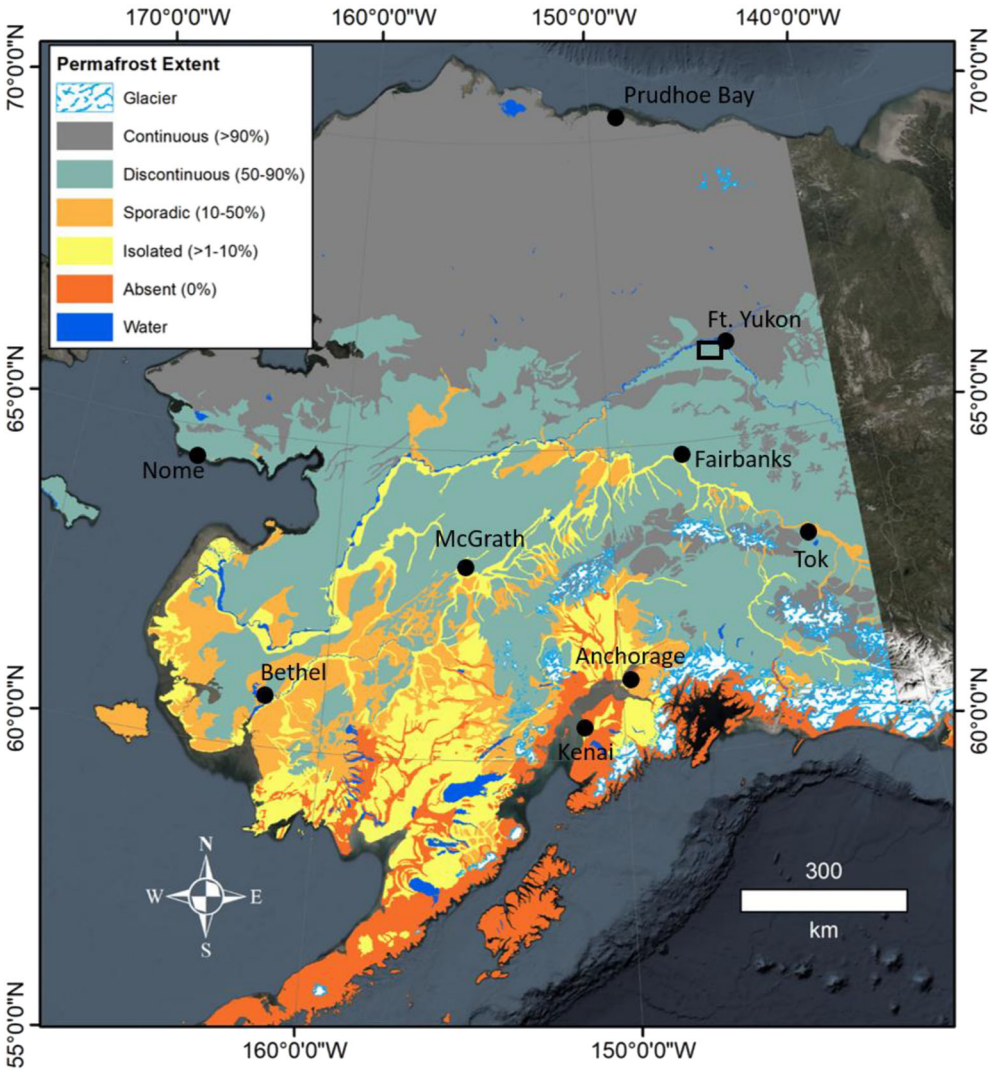

FIGURE 1 Map of Alaska showing estimates of general permafrost distribution from Jorgenson et al.,[35] and the study location discussed in this paper near Fort Yukon (black box), north of Fairbanks

winter snow cover may allow rapid refreezing during the winter.[29–31] Additionally, vegetation cover, succession, and impacts of vegetation on where snow is deposited can result in more complex ground thermal properties, spatially and temporally.[32] This complexity means that most research must include a historical context of the terrain and extensive field validation of airborne or remote sensing analyses to interpret permafrost distribution or active layer thickness and ultimately upscale local measurements across broader areas.[33,34] Previous research suggests the extent and geometry of permafrost are variable at the meter scale but much of Arctic permafrost is currently mapped laterally at the scale of 10s to 100 s of kilometers.[15,28,33–35] Airborne geophysical methods are useful for broadly mapping permafrost thickness and extent across large regions,[36] but their results can be ambiguous due to variable subsurface conditions influencing the electromagnetic (EM) response and lack of supporting ground-truth observations. Airborne surveying is also costly to perform. Permafrost thaw surrounding Arctic thermokarst lakes that cover much of central and Arctic Alaska is particularly challenging to quantify,[37] despite being an active system and one of the greatest terrestrial contributors to atmospheric methane.[38] Early research used remote sensing and ground-truthing to evaluate the presence or absence of frozen ground[39,40] and active layer thickness.[41,42] Studies have also been conducted using light detection and ranging (LiDAR) and aerial imagery to estimate the influence of biomass on ground insolation relative to permafrost occurrence.[43] Finally, remote sensing, statistical, and field validation methods have been used to estimate permafrost presence, absence, and seasonal thaw properties.[44,45]

Most of these studies note the need for more field observations to compare with remotely sensed measurements before they can be adequately projected across broader spatial extents. Geomorphological processes, vegetation succession, and succession following natural environmental processes such as forest fire activity or disturbance from infrastructure development complicate permafrost depth and extent in space and time.[15,46] In newly revegetated regions, thinner (≤30 cm) frozen horizons in late August suggest permafrost is beginning to refreeze or that these areas have just enough biomass cover and reduced solar insolation due to overburden biomass or solar aspect to maintain pockets of frozen soil in the winter.[8,28,47] Large-scale comprehensive mapping of permafrost, terrain, vegetation, and changes in these parameters would provide the opportunity to quantify dynamic relationships between these environmental conditions.

Lastly, despite the spatial and temporal variability of permafrost changes due to the variables discussed above, studies suggest that surface subsidence rates are consistent within similar geomorphological features across large geographic regions.[48,49] These complex relationships have caused international efforts to combine a range of datasets and models with the goal of predicting current and future permafrost distribution at greater accuracy based on controlling parameters. We contribute to this effort by developing an artificial neural network to predict permafrost presence, absence, and spatial distribution surrounding Twelvemile Lake within the drainage corridor of the Yukon River, Alaska. This approach allows us to explore relationships between the spatial distribution of permafrost, as determined from ground-penetrating radar (GPR) and variations in vegetation type, biomass, and multiple topographic metrics derived from satellite imagery and a LiDAR-based digital elevation model (DEM), respectively. We then use a linear regression model to explore relationships between spatial permafrost probability and seasonal thaw depth determined from frequency-domain electromagnetic induction (FDEM) field surveys. Our hypothesis was that north-facing terrain would have less solar insolation thereby reducing thermal degradation of permafrost and decreasing the depth of the seasonal freeze–thaw layer. Additionally, we predicted that vegetation cover would act as a solar barrier to thermal degradation of permafrost. Our goal was to map thaw depth, frozen lenses, and permafrost using GPR and FDEM relative to vegetation type and cover, aspect, and terrain surrounding Twelvemile Lake.

Although our approach is trained specifically to conditions at Twelvemile Lake, we provide a methodology that can be applied to accurately predict broader and increasingly complex permafrost landscapes. This study shows that both permafrost degradation and aggradation can occur over relatively small distances in space and time, that local-scale geophysical and remote sensing observations can capture these changes, and that these results can be upscaled to larger regions through coupled remote sensing, geophysics, and machine learning. Lastly, we show that this combined approach provides an opportunity to distinguish stable from unstable permafrost regions, thereby helping to refine future research objectives towards unstable regions.

2 | STUDY SITE

Twelvemile Lake is situated within the discontinuous permafrost zone, 18 km to the southwest of Fort Yukon, Alaska, and 13 km south of the Yukon River (Figure 1, black box; Figure 2). The lake is currently located near the southern boundary of continuous permafrost. However, atmospheric warming is driving the region toward a transitional permafrost landscape and will probably push Twelvemile Lake further into the discontinuous permafrost zone in the future years. Twelvemile Lake has been a site of focused research over the last decade due, in part, to its location near the boundary of continuous and discontinuous permafrost, but also because of a strong overall recession of water levels from the mid-1980s.[26–28,35,50–52] Permafrost is sporadic to nonexistent in sparsely vegetated, south-facing slopes, or within the lake talik,[50] but reaches up to 90 m thick in densely vegetated regions outside of the lake talik.[36] Despite being relatively far from the Yukon River, Twelvemile Lake still resides in the river's flood zone and has been flooded extensively in recent years (2014–2016). During nonflood stage when this study took place, the lake covered ~1.2 km^2 and it has an intermittent surface channel feature that enters from Buddy Lake to the southeast. Two apparent surface outlet channels exit Twelvemile Lake to the north and northwest. All three channels, although topographically controlled, are usually dry except for pockets of water within the beaded stream channel between Buddy and Twelvemile Lake, or during observed flooding events. Between Twelvemile Lake and Buddy Lake, frost cracks and

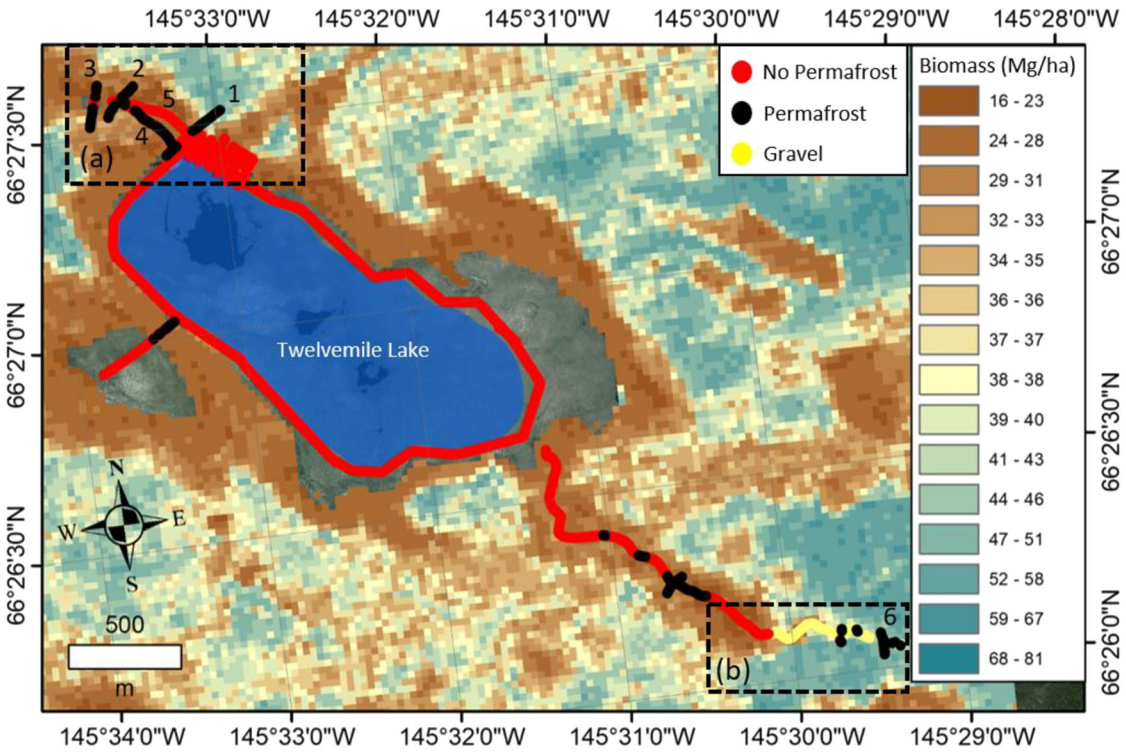

FIGURE 2 Map of Twelvemile Lake near Fort Yukon showing interpretation of GPR profiles collected in 2012 including no permafrost present (red dots), permafrost (black dots), and gravel bedding (yellow dots). The background color is approximate vegetation biomass in metric tons per hectare (Mg/ha) based on Ji et al., with brown representing minimal cover such as grasslands and dark green representing maximum cover such as forest. Bounding box (a) is the region outlined in Figures 6, 7, 8, 9, and 10 with lines 1–5. Bounding box (b) represents the Buddy Lake drainage outlined in Figure 11 and line 6 is displayed in Figure 11b

the beaded steam structure suggest the presence of massive ice or ice wedges within permafrost that impact shallow groundwater connectivity between the two water bodies[26,52] (Figure 3a,b). Twelvemile Lake is surrounded by a series of vegetation types from low grasses near the shoreline to distinct bands of willow shrubs and old-growth spruce forest at higher elevations.[28] Excavated pits and cores surrounding the lake show primarily loam over silt and into sand and gravel at greater depths (Figure 3c,d). The southeast channel between Twelvemile Lake and Buddy Lake has sand and gravel exposed at the surface in some areas. Previous local-scale work (100s of meters) has indicated vegetation succession within the dried lake channels may impact new permafrost formation and shallow groundwater connectivity.[26]

3 | METHODS

3.1 | Ground-penetrating radar

GPR is well suited for quantifying active layer thickness, seasonal thaw depths, or vertical and lateral permafrost extent because of the strongly contrasting electrical properties between thawed and frozen ground. Hand-towed GPR can be used to rapidly detect the presence or absence of shallow frozen ground across relatively large distances and at high spatial resolution, typically yielding more efficient spatial surveys when compared to other surface geophysical methods.[28] We collected a total of ~14 km of GPR profiles surrounding Twelvemile Lake in August 7–11, in 2011, April 2–7, 2012, and August 28–31, 2012, during the low water period before large-scale flooding events were observed in 2014–2016.[28] However, we relied on the most extensive dataset collected in August 2011 for comparison with the other geophysical results and machine learning in this study.

We used a Geophysical Survey Systems Inc. (GSSI) SIR-3000 control unit coupled with a GSSI model 5,103 400-MHz bistatic antenna and GSSI model 3,207 100-MHz bistatic antenna to survey the near-surface geology, seasonal thaw depth, depth to permafrost, or seasonal freezing in areas where permafrost is absent in the near surface. We hand-towed each antenna at ~0.5 m/s oriented perpendicular–broadside to the data collection direction with traces lasting between 80 and 600 ns and 1,024–2,048 16-bit samples per trace, with both time window and sampling rate dependent on specific profiles we collected. Profiles were recorded with range gain, band pass filtering, and stacking to reduce noise and improve signal to noise ratios, particularly for flat lying reflectors. Ten-meter distance marks measured with a tape measure were used to distance-normalize the profiles. We estimate a 0.5 m lateral uncertainty following distance normalization. Following distance normalization, a post-stack variable velocity migration for time–depth conversion was performed using GSSI proprietary

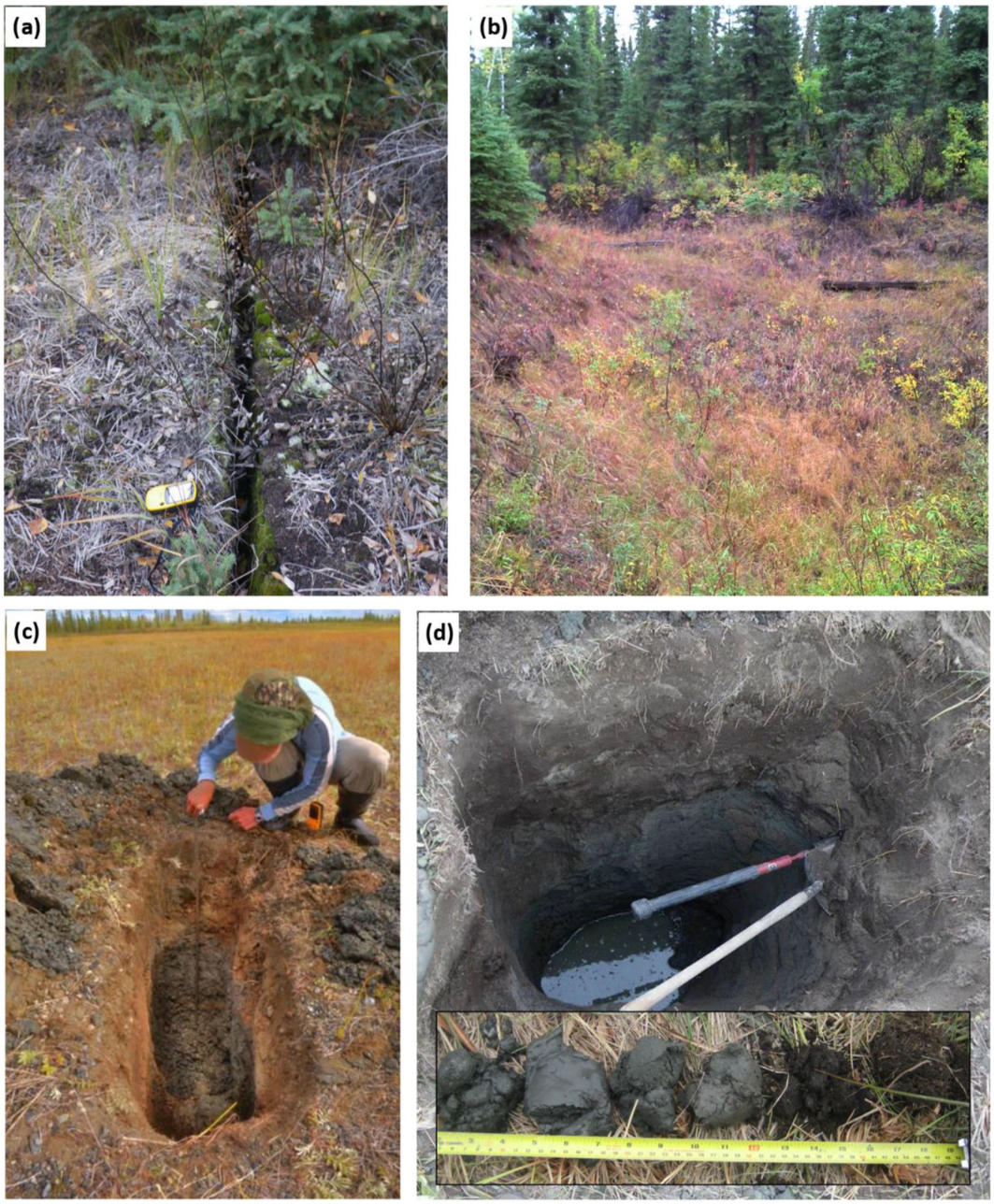

FIGURE 3 Observations and ground-truth used for GPR interpretations at Twelvemile Lake. (a) Frost crack observed in the southeast region of Twelvemile Lake in a region where permafrost was interpreted from GPR, a shallow pit, and frost probing. (b) Drainage inlet between Buddy Lake and the southeast corner of Twelvemile Lake near the frost crack showing the depressed thaw zone of the beaded channel. (c) Excavated pit near where a steel pipe was installed laterally at 1.17 m depth into the sediment. This pit was used to estimate the near surface relative permittivity (ϵ_r) based on the known depth of the installed steel pipe and the calculated radio wave velocity. (d) Pit excavated near Twelvemile Lake showing the complex sedimentary structure of fine-grained and saturated silt, wet sands, and surface peat (inset photo, left to right) with water table at the pit bottom

software through hyperbola matching to estimate relative permittivity and associated wave velocities spatially and with depth. Each 10-m mark location was also recorded with a handheld Garmin GPSMap62 STC which revealed an ~ 1-m spatial uncertainty relative to measured distances. Ground-truthing of the GPR data was conducted by the excavation of shallow (2–3 m) sediment cores and dirt pits or via frost-probing (e.g. Figure 3c,d). We also installed a steel pipe within the sidewall via sledge hammer of one extracted pit at 1.17 m depth along the pit sidewall and collected a common-offset GPR profile over the pipe to determine radio-wave velocity and associated relative permittivity (ε') of the active layer (Figure 4) based on the known depth of the pipe and the following equations:

$$V = \frac{c}{\sqrt{\acute{\varepsilon}}} \quad \text{(Eq1)}$$

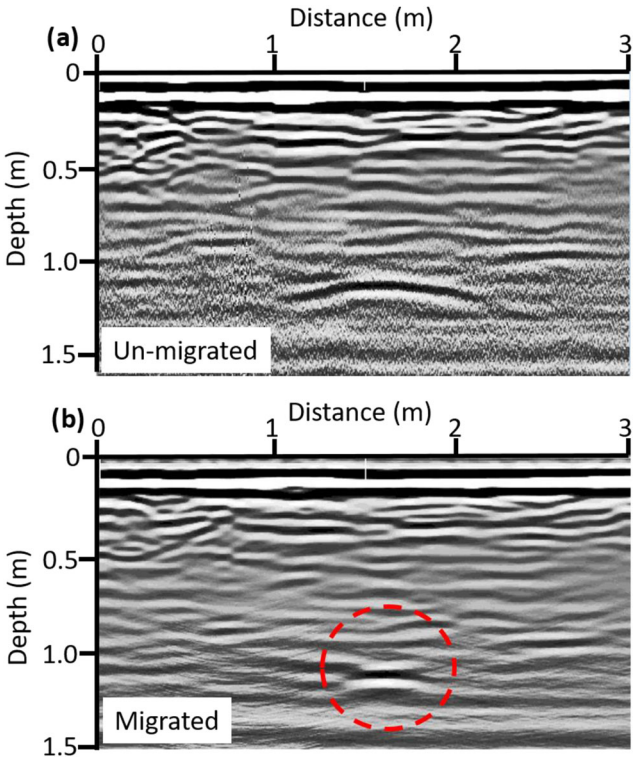

FIGURE 4 (a) Unmigrated 400-MHz GPR profile showing 1.5-cycle + – + (positive) triplet caused by a steel pipe buried at 1.17 m depth. (b) Migrated 400-MHz GPR profile showing the same 1.5-cycle triplet collapsed using a value of ε_r = 19

$$d = \frac{(TWTT * V)}{2} \quad \text{(Eq2)}$$

where V is velocity (m/ns), c is the speed of light, d is depth (m), and TWTT is the two-way travel time (ns). The installed pipe was slightly oblique to the direction of radar profiling, resulting in a wide hyperbola that was difficult to fully collapse. However, given the known depth and that a ε' of ~19 resulted in the most collapsed hyperbola, we assumed this value at the test site. Active layer ground-truth and migration calculations suggested ε' ranged between 14 and 26 at other locations. Within the shallow thawed region (50 ns TWTT) this equates to a 0.5-m difference in depth between ε' of 14 and 26. We used the waveform polarity of reflections to interpret relative changes of ε' between layers.[28] For example, a + – + (positive) horizontal and continuous triplet horizon at the bottom of the seasonal thaw layer suggests an abrupt transition from higher to lower ε' with depth, a likely scenario between a thaw zone above and permafrost or frozen layer at some depth. Differences in ε' of water (~80), permafrost (~5.3), ice (~3.2), air (1), and a wet active layer (~14–26, depending on moisture content) provide enough contrast to interpret changing dielectric properties at horizons and discrete events. These GPR data were collected with other geophysical measurements to compare the effectiveness and efficiency of mapping permafrost using different methodologies.[28] Corroborating results between other geophysical methods and GPR is discussed elsewhere,[28] providing a high level of confidence in our GPR interpretations. This confidence allows further analysis of our GPR results relative to the terrain and biomass surrounding Twelvemile Lake. All described profiles have time ranges labeled as TWTT unless otherwise noted and depths based on an ε' of 19.

3.2 | Frequency-domain electromagnetic induction

Electromagnetic methods have been used to detail permafrost features in cold regions for decades.[53] Airborne-based transient EM imaging has been applied in the Yukon Flats area to map the horizontal and vertical extent of thicker permafrost layers,[36] although finer scale and partially frozen near-surface permafrost features are not typically well resolved from the air.[54] However, ground-based electromagnetic tools such as FDEM have been shown to capture meter-scale, thin new permafrost zones in the receded Twelvemile Lake margin,[28] showing good agreement with more commonly used GPR methods.

Like hand-towed GPR, hand-carried FDEM is a highly mobile geophysical method that exploits the contrasting electrical properties of frozen and thawed ground to map near-surface permafrost distributions along two dimensional (2D) transects. A primary EM field generated by the FDEM transmitter loop is used to induce secondary EM fields in the subsurface that are directly related to bulk electrical conductivity of the soils. As the method can operate across a range of frequencies, depth-specific resistivity structure information can be recovered, where lower frequencies and higher frequencies generally sense larger/deeper or smaller/shallower volumes, respectively. FDEM has recently grown in popularity for mapping shallow groundwater flow paths and groundwater/surface water exchange dynamics,[55–57] although applications to cold regions are still relatively novel.

As detailed in Briggs et al.,[28] we collected FDEM in the "outlet" zone of Twelvemile Lake using the multifrequency GEM-2 instrument (Geophex, Inc.) operated over seven frequencies from 1,530 to 93,090 Hz with 1.66 m coil separation. Unlike the apparent FDEM bulk soil resistivity data reported previously,[28] we recovered "true" bulk values from the raw instrument quadrature data using the GCM module in Aarhus Workbench software (Aarhus Geosoftware). We assume a 10% error for the raw data, which was resampled to 1-m spatial intervals using a 3-m moving average window before calculating the 18-layer inversions. The realized depth of investigation for this survey was ~ 4 m as indicated by the Workbench software, although this depth was variable in space.

3.3 | Terrain and biomass analyses

We compare a 2.5-m-resolution airborne-derived LiDAR DEM with vertical positional accuracy of 0.10 m to permafrost extent and seasonal freeze estimated from GPR interpretations surrounding Twelvemile Lake.[58] We used the DEM to determine aspect, assuming

this variable along with latitude and terrain shadowing most heavily influences incoming solar insolation. We modeled total insolation (I_t) acquired for each pixel in the image between January 1, 2011 and December 31, 2011. This calculation, which was derived from previous work,[59–61] estimates insolation from a hemispherical viewshed algorithm:

$$I_t = Dir_t + Dif_t + Ref_t \quad \text{(Eq3)}$$

where units are Wh/m^2, Dir_t is total direct insolation, Dif_t is total diffuse insolation caused by scattering, and Ref_t is the reflected insolation caused by surface reflectivity and terrain features. Unfortunately, our calculation does not include Ref_t because a good estimate of this value is not available at Twelvemile Lake. We assume the area is snow-covered during winter, which would result in albedo of ~90%. However, as summer progresses, bare ground and vegetation are exposed, both of which have a lower albedo (~30–70%) resulting in greater solar absorption. We therefore consider the combination of direct and diffuse insolation as a first-order conservative approximation and assume that if we included Ref_t, then I_t would increase.

The LiDAR-derived DEM is a bare earth model with vegetation removed through standard LiDAR processing techniques. We expected some discrepancies between total insolation derived from the bare earth model versus values derived from the raw LiDAR dataset, particularly in areas where thick vegetation (e.g., biomass) is removed as part of the bare earth processing. Therefore, along with the DEM analysis, we compared permafrost extent interpretations from GPR and FDEM to an available 30-m resolution biomass dataset derived from Landsat imagery from a previous study, across the Yukon River watershed.[58,62,63] The biomass dataset was derived from spectral and statistical analyses of five overlapping Landsat 5 Thematic Mapper images acquired in 2008 and field biomass measurements for ground-truthing. We also used the 2.5-m-resolution airborne LiDAR bare earth model described above and a first return DEM to estimate vegetation height for comparison to derived biomass calculations. Processing and analysis of the imagery to derive biomass is provided by referenced work.[58] However, generally, above-ground biomass defined for our analysis is the sum of tree, shrub, coarse woody debris, and understory mass.

3.4 | Artificial neural network

We developed a MATLAB-based artificial neural network (ANN) to infer spatial patterns of permafrost distribution where observational data are scarce. Similar machine learning and remote sensing approaches have been successfully used to identify various permafrost characteristics in Arctic environments, including ice wedge polygon presence and morphology,[64–73] growth of thermokarst lakes,[74,75] and coastal permafrost erosion.[76,77] Our ANN is a supervised machine learning classification algorithm that generates a probability of permafrost existence based on the datasets described above. More specifically, we use a pattern recognition two-layer feed-forward neural

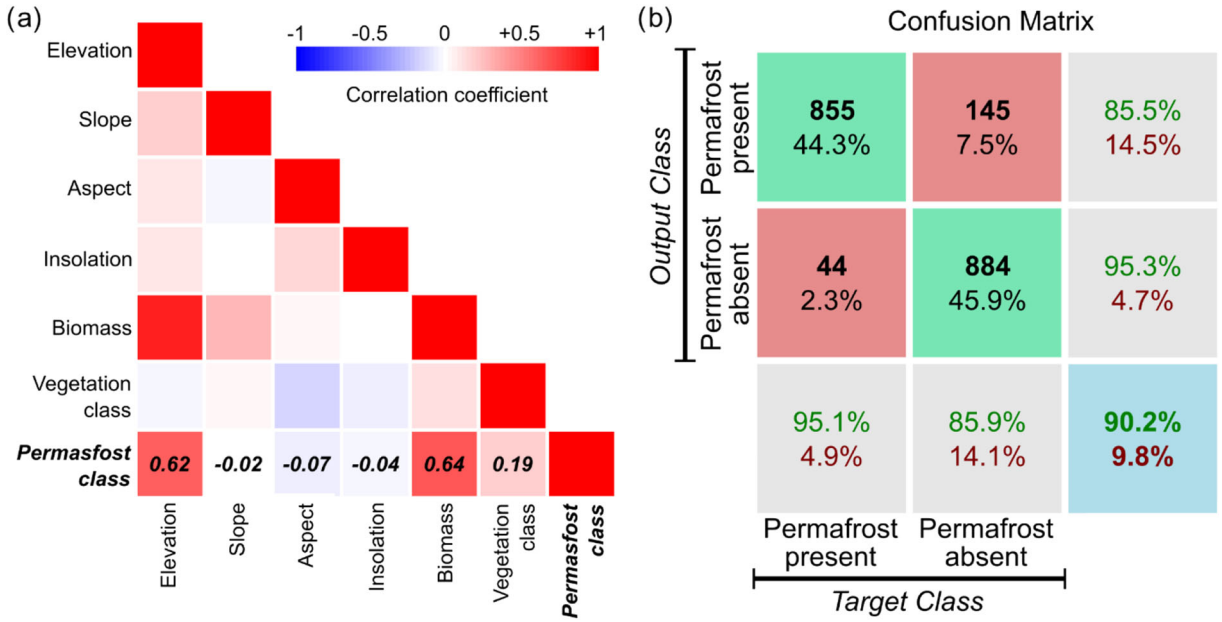

FIGURE 5 (a) Correlation coefficient matrix for input variables and binary permafrost class. No one variable strongly correlates with permafrost class. We omit elevation and slope, metrics that are redundant and provide the weakest correlation, respectively, from ANN training. (b) ANN confusion matrix combining final results for training, validation, and test samples. A confusion matrix allows visualization of the performance of the ANN to determine if the algorithm is confusing the two classes, where each row represents the instances in an output/predicted class and each column represents instances in the target/actual class. Green squares denote number of correct responses, and red squares denote number of incorrect responses. Lower right blue square denotes overall model accuracy. Bordering squares denote percentage true match (green) and false positive and negative (red) output

network with single input, hidden, and output layers. The hidden layer consists of 18 sigmoid transfer function neurons and the output layer consists of two softmax transfer function neurons representing output classes of "permafrost" or "no permafrost." The softmax function maps the network output to a probability distribution over the predicted output classes.

The training dataset for the ANN consists of 1,928 interpretation points of permafrost presence or absence derived from GPR transects. Model probabilities are generated in a continuum across the landscape surrounding Twelvemile Lake at 2.5 m resolution based on input data listed in Figure 5a. Prior to training the ANN, we assessed Pearson correlation coefficients between continuous variables and point-

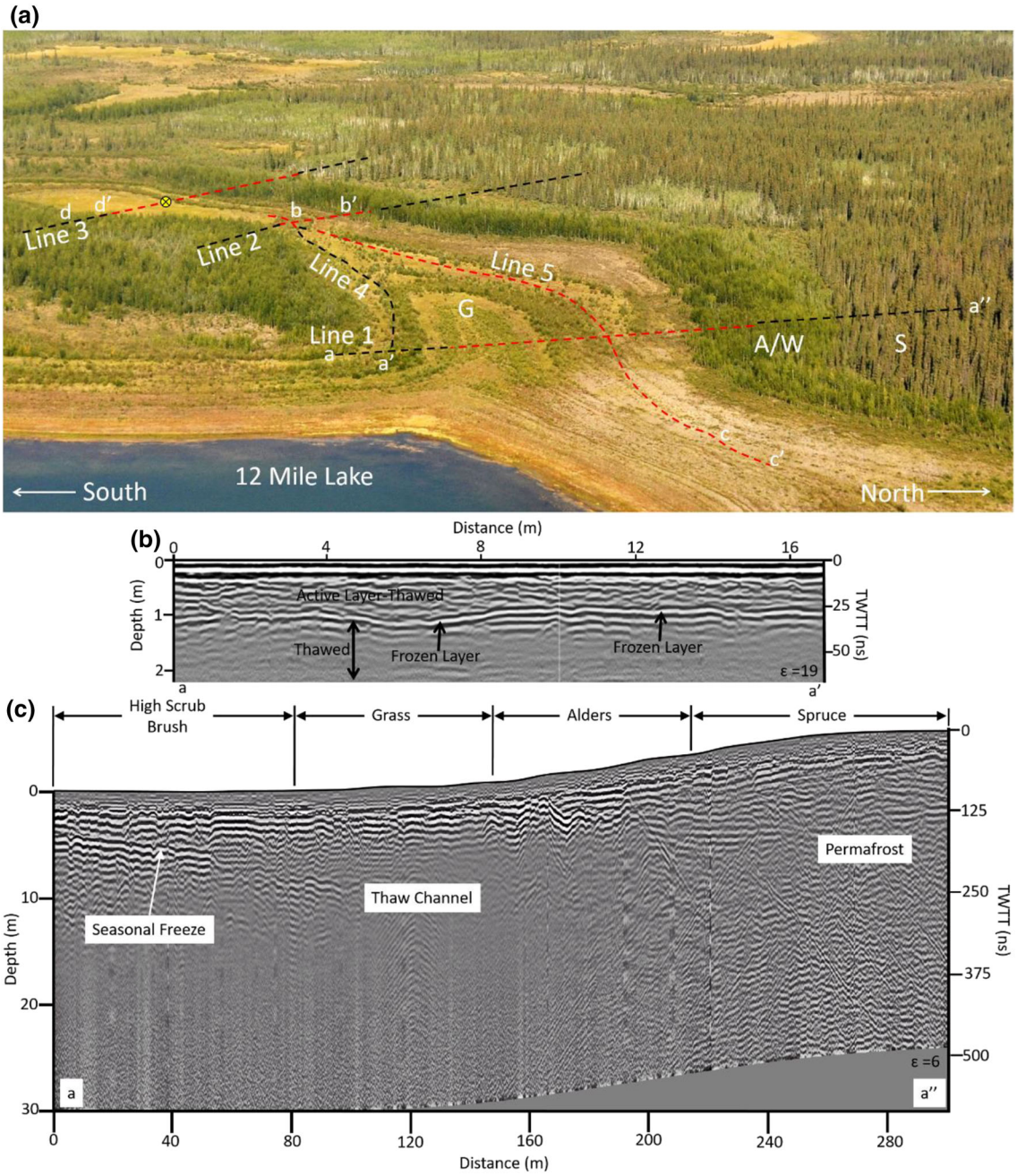

FIGURE 6 (a) Aerial photo (photo: Jay Nolan) of the northwest outlet of Twelvemile Lake showing approximate locations of each GPR profile (dashed lines) collected in 2012 (lines 1–5) and sections of each profile (a–a′, a–a″ b–b′, c–c–, d–d′, and a yellow bulls-eye) discussed within the paper and displayed in Figures 6, 7, 8, and 9. Red dashed lines are interpreted as areas without permafrost and black lines are interpreted as areas that have a permafrost or a thin refreezing layer. Vegetation cover across the study region include grasslands (G), aspen and willows (A/W), and spruce trees (S). (b) 400-MHz GPR profile collected in April 2012 from a to a′ along line 1 showing a frozen layer within the thawed active layer. The frozen layer is probably remaining from winter freeze but survives late into the summer due to vegetation succession. (c) 100-MHz GPR profile collected from a to a″ along line 1 showing seasonal freeze, the thaw channel, and permafrost regions corresponding to biomass vegetation cover

biserial correlation coefficients between continuous variables and the binary classification data interpreted from GPR surveys. All terrain and biomass input variables collected for this study were used for this analysis. We found no statistically significant difference in Pearson and point-biserial correlation coefficients and therefore report only Pearson coefficients (Figure 5a). Although some input variables displayed stronger correlation than others, our linear regression analysis indicated that no one variable can adequately describe patterns of permafrost distribution alone. After we determine permafrost, we use FDEM in conjunction with the ANN model to predict thaw depth or depth to permafrost.

Training, validation, and testing followed *k*-fold cross-validation, in which samples were randomly divided into training (70%; 1,350 samples) and validation (15%; 289 samples) groups over multiple iterations until there was no further improvement in model performance. An additional sample group (15%; 289 samples) was set aside for an independent test of network generalization. This cross-validation approach ensured that all available data resources were used for training, validation, and testing, improving the overall accuracy and generalization of the final model.[78] Our final training produced an ANN with overall accuracy of 90.2% (Figure 5b). The ANN model provides far greater predictive accuracy than linear regression in this context and is therefore an important asset for permafrost mapping. We therefore apply this approach to develop the permafrost probability map results described below.

4 | RESULTS AND DISCUSSION

4.1 | Ground-penetrating radar

Maximum depth of penetration for the 400-MHz data ranged between ~1 and 3 m whereas the 100-MHz antenna successfully imaged structures at maximum depths reaching 5–25 m. Both antennas had high attenuation or noisy results within the grassland-covered channels or near open regions surrounding Twelvemile Lake. We interpret these regions to be low-resistivity (100–150 Ω.m) zones with high silt or free water content that caused signal volume scattering (Figure 6a) based on previously conducted electrical resistivity imaging.[28] Maximum penetration for both antennas occurred under areas covered by willow and spruce trees at higher elevations. A continuous negative triplet horizon at 20–40 ns TWTT also occurred within the willow and spruce trees (Figure 6b), which we interpreted to be the transition layer between the bottom of the seasonal thaw and the top of the permafrost.[28] In thickly vegetated regions we generally expect thin seasonal thaw over thick permafrost due to

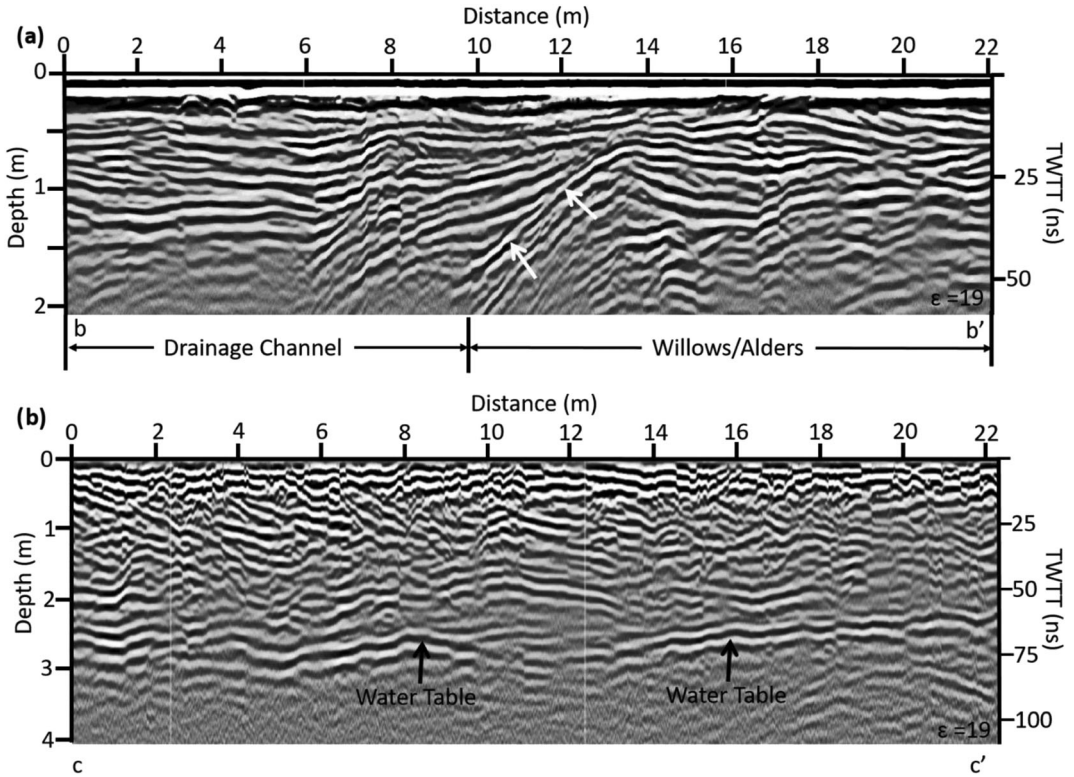

FIGURE 7 400-MHz profiles showing stratified sands and gravels and a water table. (a) 400-MHz profile along line 2 (b to b′) showing a transition from stratified sands and gravels which transition into an unconformity against the channel (white arrows). (d) 400-MHz profile collected along line 5 (c to c′) showing the water table (black arrows) at 2.5 to 3 m depth paralleling the shoreline of Twelvemile Lake

vegetation cover protecting the ground from direct solar insolation, recognizing that snow cover can also influence ground thermal properties. Signal penetration depths up to 25 m deep within the spruce forest with the 100-MHz antenna (Figure 6c) suggest the ground was well-drained and highly resistive in this region, which is typically representative of thick permafrost. Ground-truth and galvanic resistivity profiles confirmed this interpretation.[28] We calculated ε' from ground-truthing via manual frost probing to be highly variable, ranging between ~5 and 26 in dry and frozen ground or wetter regions, respectively. Similar values have been recorded in other studies.[79–83] The variability of ε' is primarily dependent upon the water content. This can result in significant depth calculation uncertainties because water content observed from ground-truth was highly variable in sediments surrounding Twelvemile Lake.

Horizontal or subhorizontal and relatively continuous reflectors within GPR profiles are interpreted as either sedimentary structures (Figure 7a), the water table (Figure 7b), the abrupt transition from seasonal thaw to permafrost, or a thin frozen layer within the active layer, which formed during the winter and has yet to fully thaw (Figure 6b,c). Our interpretation depends on the GPR signal phase change at each horizon,[80] the location of the event or horizon relative to surface observations (such as vegetation cover or proximity to Twelvemile Lake), and available ground-truth information. For example, on line 2 located in the northwest corner of Twelvemile Lake (Figure 6a) we noted stratigraphic horizons that thinned and were bisected at an unconformity near the edge of the northwest channel (Figure 7a, arrows). This unconformity suggests a change in geological structure. The proximity to the channel edge at the surface suggests that we located the edge of a paleochannel that has filled over time through natural processes. The water table or transition from thawed to frozen ground exhibit similar characteristics to each other. For example, both are typically flat-lying and continuous in GPR profiles collected over consistent terrain. However, their triplet responses are opposite; that is, a water table below moist sediment displays a positive triplet response (Figure 7b, arrows) and permafrost below moist thawed ground exhibits a negative triplet response (Figures 8a,b).

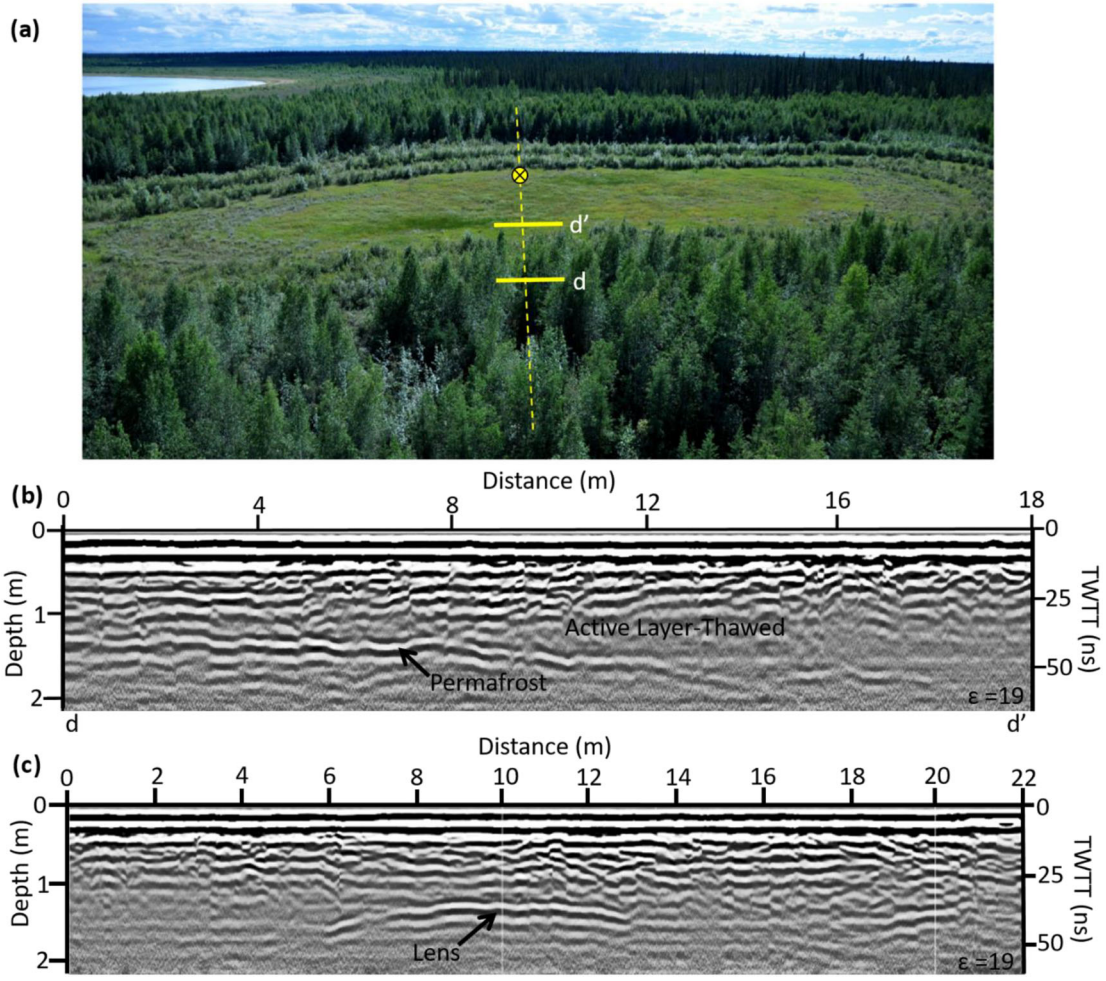

FIGURE 8 Aerial photo and GPR results from line 3. (a) Aerial photo of approximate GPR line 3 location collected at the northwest channel of Twelvemile Lake. (b) 400-MHz profile from d to d′ showing the thawed active layer over permafrost. The active layer-permafrost horizon dips to greater depths as the profile traverses into the thaw bulb of the drainage channel. (c) 400-MHz GPR profile showing a well-drained sand lens situated within predominantly wet fine silt in the northwest outlet of Twelvemile Lake. Lens location is marked in (a) via the circle with an x

Interpretations become more difficult in regions where ground-truth is unavailable, where surface observations do not provide potential clues, or where subsurface reflections are complex. For example, one short horizon noted on line 3 in the northwest channel (Figures 6a and 8a,c; yellow circle X) presented a positive triplet, suggesting a transition from higher to lower ε'. In thickly vegetated regions (e.g., Figure 3b, spruce and thick understory in photo background) our typical interpretation for this horizon would be permafrost below thawed ground. However, this horizon was located within the channel and was covered by minimal vegetation, an area we would expect to have minimal to no permafrost (e.g., Figures 6a and 8a, grassland). In this specific case, frost probing revealed that this horizon was a thin and well-drained sand lens surrounded by wet silt. The phase response would be similar for permafrost or a well-drained sand lens under wet silt.

4.2 | Frequency-domain electromagnetic induction

In general, thin and discontinuous near-surface permafrost lenses were mapped with FDEM[50] in the lake outlet meadow area and associated with bands of dense willow shrub vegetation (Figure 9).[28] The permafrost lenses presented as moderately resistive anomalies along largely low-resistivity profiles, indicating a predominance of unfrozen wet silt. Strongly resistive profiles were associated with the spruce forested areas and interpreted as thick, older permafrost below dry thawed ground. Resistivity thresholds to indicate partially frozen lenses and solid permafrost were estimated at 300 and 380 Ω.m, respectively, based on cross referencing the inverted FDEM data with known zones of each frozen ground type. Those thresholds were utilized in the ANN-based analysis as described below.

4.3 | Terrain and biomass analysis

The airborne LiDAR DEM surrounding Twelvemile Lake provides a mechanism to study the potential influence of solar insolation on bodies of discontinuous permafrost. The DEM provides a general understanding of hydrological controls to the water budget via the inlet from Buddy Lake and outlets located at the northwest corner of Twelvemile Lake (Figure 10a). An aspect analysis of the DEM in the northwest corner of Twelvemile Lake shows some local correspondence between northward or southward ground orientation relative to regions interpreted to have permafrost or not, respectively (Figure 10b). This is expected considering north-facing slopes should receive less solar insolation per unit of time relative to south-facing slopes. Our modeled solar insolation over the course of 2012 (Figure 10c) supports this relationship in most cases. For example, the southern half of lines 1, 2, and 3 (Figure 6a) all exhibit permafrost or a thin frozen layer (Figure 10a), all face northward (Figure 10b), and all have lower modeled solar insolation values calculated from the DEM (Figure 10c), relative to the northern section of each line. Likewise, line 4 exhibits permafrost or a thin frozen layer and receives less direct solar insolation than line 5 due to its north-facing aspect. In contrast, line 5 faces south and shows no evidence of permafrost or frozen layers within the near (1–3 m) surface.

Discrepancies in this analysis occur on the northern end of lines 1, 2, and 3. Permafrost or frozen layers exist in these regions. However, the north ends of all three lines dominantly face south and therefore receive significant solar insolation relative to a north-facing slope. We attribute this discrepancy in permafrost existing under south-facing slopes to be dominantly influenced by biomass cover. For example, the last 120 m of line 1 exhibits thick permafrost according to ground-truth data, our GPR interpretations, and geophysical results from previous research[28] (Figure 6a,c). Although this region of line 1 faces south, biomass ranges between ~50 and 110 Mg/ha in the form of thick willows and spruce trees, which protect the ground from solar heating (Figures 6a and 10d). A similar, albeit weaker case can be made for the northern end of lines 2 and 3 because the biomass is thin (10–15 Mg/ha) in these regions, although it is still thicker than the grasses that dominate the center of the northwest channel (1–5 Mg/ha). Extensive ground-truth efforts, electrical resistivity surveys, and numerical modeling efforts simulated thermal properties of lines 1, 2, and 3.[28] The GPR data presented here were collected in conjunction with Briggs et al.[28] Each of these datasets presents a compelling case suggesting that thin and pocketed permafrost aggradation along

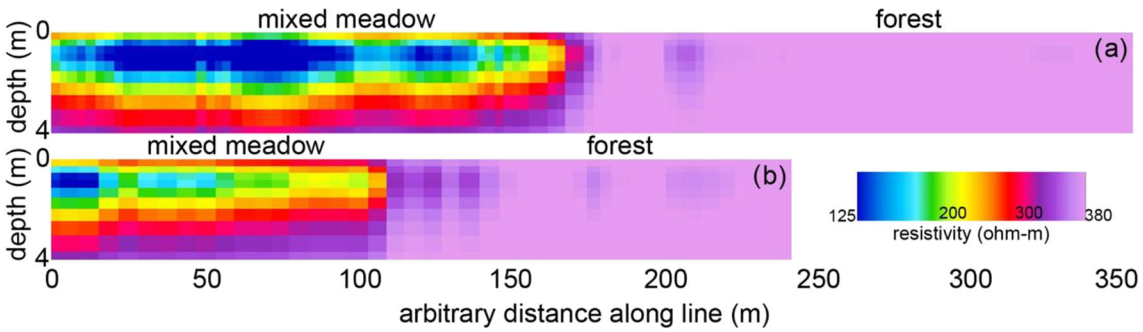

FIGURE 9 Inverted FDEM data collected along line 1 (a) and line 2 (b) show systematic reductions in soil resistivity from the forested areas that are underlain by permafrost, to the thawed mixed meadow areas within the margin of the receded Twelvemile Lake

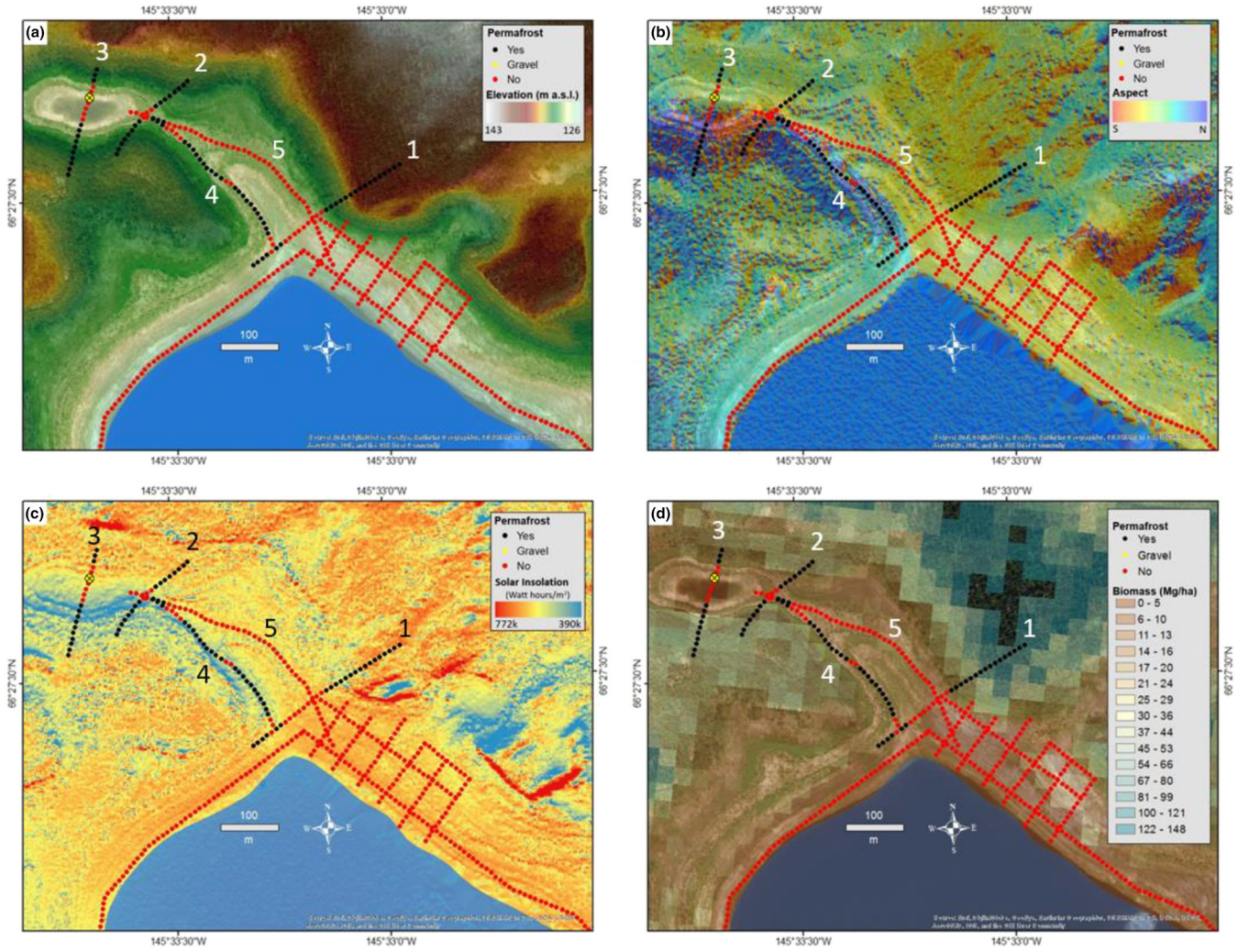

FIGURE 10 Series of remote sensing images comparing GPR profile interpretations relative to elevation, aspect, solar insolation, and biomass cover. (a) High-resolution (2.3 m) DEM over a worldview image of the western drainage of Twelvemile Lake (bounding box (a) in Figure 2) showing interpretations from GPR profiles exhibiting either permafrost or frozen ground (black dots) or regions without evidence of either (red dots). (b) Calculated aspect raster from the DEM showing its relationship to GPR interpretations. Note that much of the north-facing slope exhibits evidence of frozen ground or permafrost. (c) Modeled 2012 solar insolation raster from the DEM showing its relationship to GPR interpretations. Note that much of the lower solar insolation regions correspond to the north-facing aspect and associated permafrost or frozen ground interpretations. (d) Biomass cover calculated by Ji et al., in comparison to GPR profile interpretations. Note, the south-facing slopes that exhibit evidence of frozen ground or permafrost generally have higher biomass which acts as a thermal barrier to solar insolation

channel margins is controlled primarily by biomass cover from vegetation succession of grassy open areas to woody shrubs (e.g., Figure 6a, Line 4 and the southern half of Line 1).

The southeast inlet represents another case study showing similar results to those derived from the southwest channel of Twelvemile Lake. Within this channel we noted permafrost was prevalent in the higher biomass regions dominated by spruce forest (Figure 11a). For example, biomass over a 400-MHz GPR profile that we collected across and oriented perpendicular to the channel (Figure 11b, a to a′) ranged from 90 to 140 Mg/ha, significantly higher than the open regions surrounding Twelvemile Lake. This GPR profile (Figure 11b) revealed a strong continuous negative triplet horizon at 25 ns TWTT along the entire transect length, which we interpret to be the top of the permafrost table below a thin (~1 m) thaw layer. Frost probing confirmed this interpretation. Unfortunately, much of the GPR data collected within the inlet between Buddy Lake and Twelvemile Lake were challenging to interpret because the subsurface structure was complex with numerous diffractions, short or relatively discrete horizons, and unconformities with both positive and negative triplet sequences. Field observations revealed multiple exposed gravel beds on the surface within the drainage channel between Twelvemile Lake and Buddy Lake, suggesting that this channel was a relatively high-energy fluvial paleochannel in the past[84–86] and that it is sporadically active during Yukon River flooding events.[25] We therefore interpreted these stratigraphic horizons to be gravel beds as opposed to permafrost or no permafrost (Figure 11a). We note that the interpreted

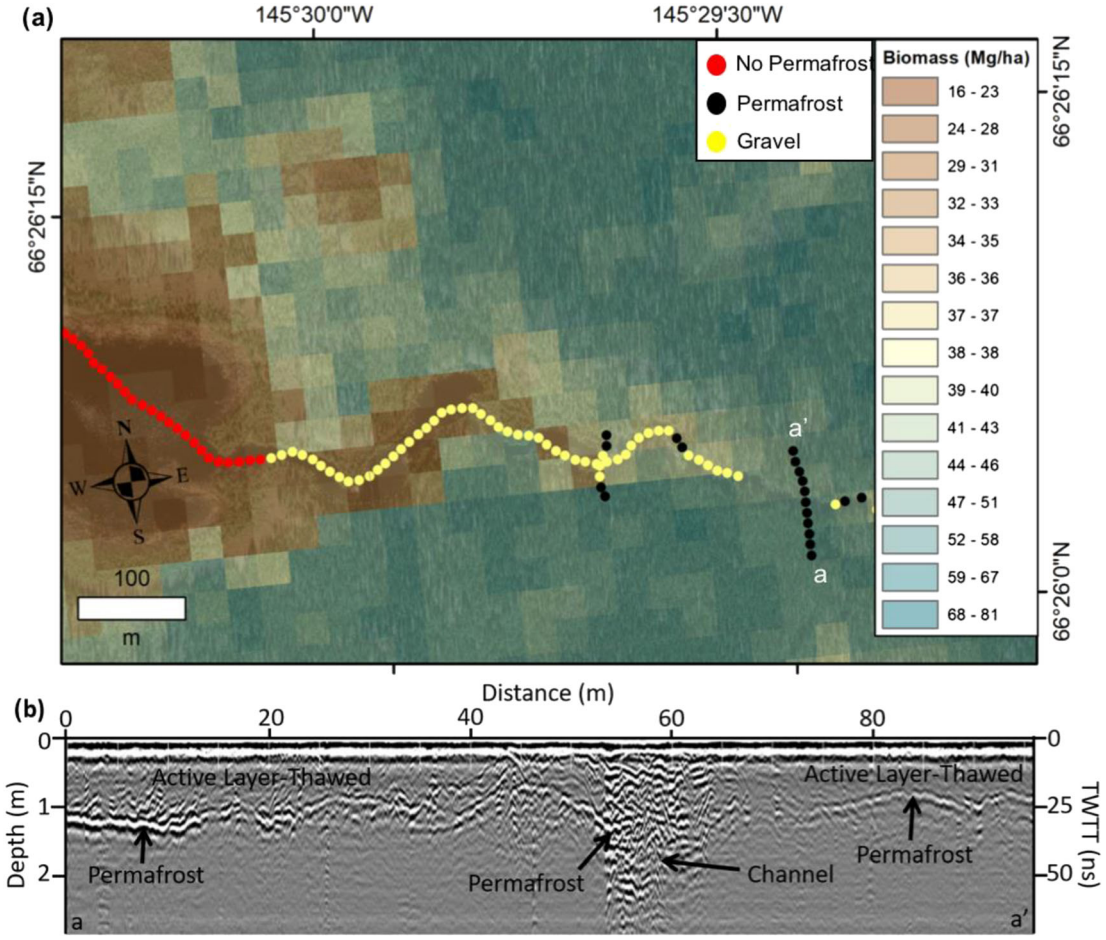

FIGURE 11 Map of biomass cover and a GPR profile (a to a′) collected across the Twelvemile Lake inlet (a) zoom of region (b) in Figure 2 compared with GPR interpretations collected in the same region showing biomass in comparison to GPR interpretations of regions with evidence of permafrost, no permafrost, or gravel fill from fluvial processes. GPR interpretation is over vegetation biomass raster from Ji et al., with brown representing minimal cover such as grasslands and dark green representing maximum cover such as spruce forest. (b) 400-MHz GPR profile collected along a to a′ showing a strong permafrost horizon and gravel channel. The permafrost potentially acts as a subsurface barrier to groundwater flow between Buddy Lake and Twelvemile Lake

permafrost horizon from Figure 10b continues across the gravel channel, suggesting that permafrost may influence near-surface hydrologic connection between Buddy Lake and Twelvemile Lake, which supports existing conceptual models.[25]

A quantitative analysis of our data suggests solar insolation and biomass influences on permafrost and refreezing ground could be distinguished from each other. Yet, we also found that neither is a good sole indicator of permafrost presence or absence across large geographic regions. These observations agree with our correlation analysis (Figure 5a). For example, the mean distribution of biomass over all GPR-interpreted regions in our data exhibiting or not exhibiting permafrost were nearly identical (Figures 12 and 13; ~20 Mg/ha). Permafrost-rich regions did have a skewed tail towards greater biomass although not enough to be statistically significant from regions with no permafrost. However, a multivariable analysis at the local scale showed expected quantitative patterns. For instance, we compared the modeled solar insolation and biomass to permafrost interpretations across line 1 at the northwest corner of Twelvemile Lake (Figures 6 and 14). The southern end of this line exhibited a mostly continuous thin frozen layer between 0 and 60 m distance. This region contained low biomass values (i.e., grasslands with some alders), which provide minimal protection from incoming solar radiation, but it also experienced low modeled solar insolation due to its north-facing aspect (Figure 10c). Between 70 and 160 m, low biomass persisted, but a south-facing aspect caused higher modeled solar insolation values. This region displayed no evidence of permafrost or a buried frozen layer. At ~200 m, modeled solar insolation decreased while biomass cover increased. This region corresponded with the reappearance of permafrost in GPR profiles. Finally, predominantly high solar insolation values between 220 and 320 m due to a south-facing aspect suggests permafrost should not exist in this region if aspect alone is used to estimate permafrost distribution. However, GPR profiles show thick permafrost throughout this section of line 1. We suggest that the high biomass values (i.e., spruce trees with thick understory) protect this permafrost-rich region from thermal erosion processes.

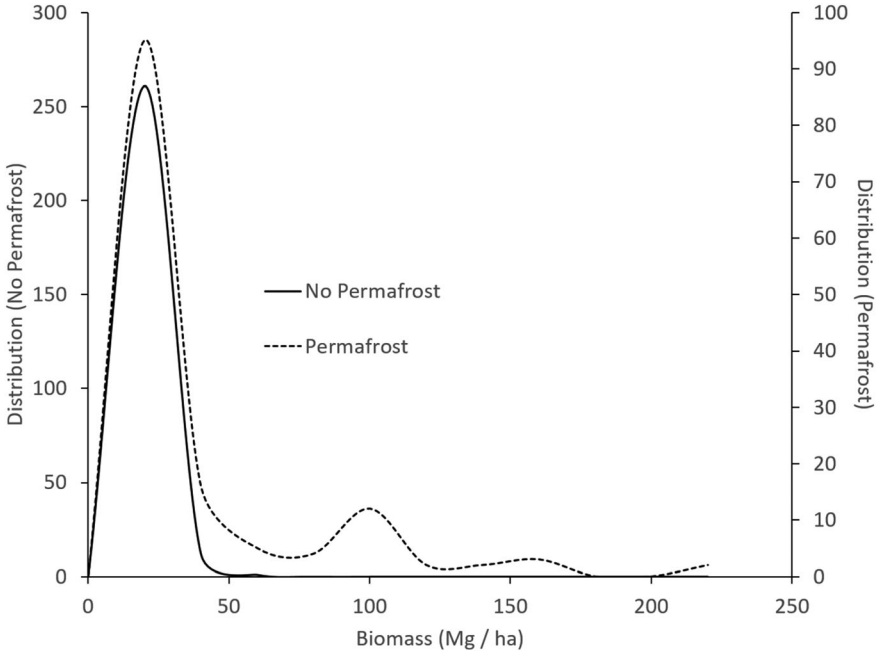

FIGURE 12 Density curves of biomass over regions interpreted by GPR to have permafrost or not have permafrost surrounding Twelvemile Lake. Note the nearly identical modal values of both curves but a skewed distribution towards higher biomass values with the curve representing regions which exhibited permafrost in GPR profiles

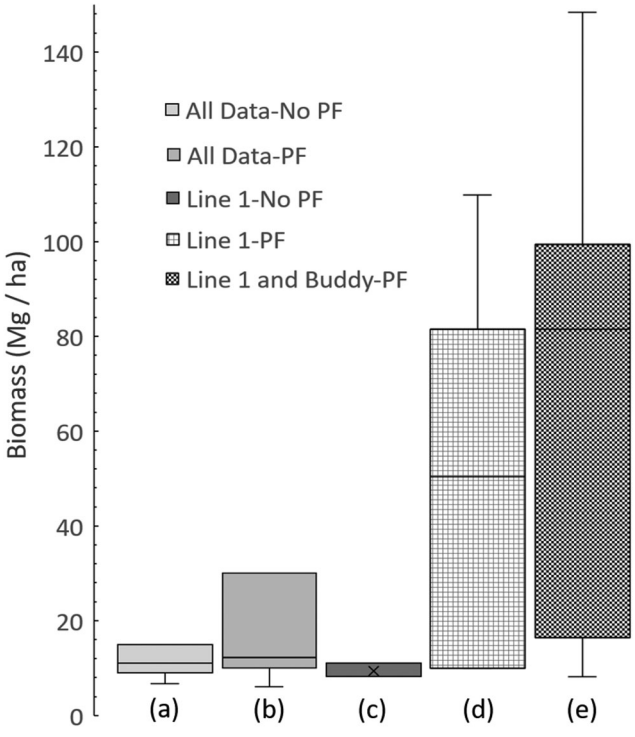

FIGURE 13 Box and whisker plots showing biomass over all regions interpreted from GPR to not have permafrost (a) or have permafrost (b), from line 1 to not have permafrost (c), from line 1 to have permafrost (d), and from line 1 and transects between Buddy Pond and Twelvemile Lake to have permafrost (e). Note, the regions with no permafrost typically have less than 15 m/ha whereas regions exhibiting permafrost have a greater range of biomass cover but far higher median values

These results emphasize that both aspect and biomass are important controls on permafrost and that thick vegetation has a stronger ground thermal forcing than aspect for south-facing slopes by reflecting or absorbing solar radiation, thereby reducing seasonal or permafrost thaw. Our results also suggest that regions of even relatively low biomass, such as willow and alder trees within open grassland, can support pocketed permafrost aggradation. These dynamic terrain and biomass controls on permafrost thaw are challenging to interpret using traditional linear statistical models. To address this, we used an ANN approach to quantify how these variables interact to control permafrost thaw and map spatial probabilities for the extent of permafrost.

4.4 | ANN-based permafrost probability maps

Results from our ANN algorithm indicate high permafrost probability in regions distal from Twelvemile Lake dominantly in areas that are north facing or that have high biomass cover (Figure 15a). We report ANN results as a permafrost probability map, where high values denote 100% probability of permafrost existence and low values denote 0% probability of permafrost. Locations with low permafrost probability tend to occur within and along the banks of Twelvemile Lake and surrounding ponds, streams, and other depressions with low relief and low biomass production. High permafrost probabilities generally occur in regions with relatively higher relief and biomass productivity, in agreement with field observations. In general, the probability of permafrost increases sharply within ~150 m from shorelines, but low probabilities are more pervasive near the inlet from Buddy Lake and the northwest outlet. Permafrost probability is generally lower to the west and southwest, corresponding with a greater abundance of small, low-relief basins.

ANN probabilities reveal greater complexity of permafrost distribution in the northwest outlet (Figure 15b), probably reflecting the complex topography, subsurface geology, and evolving vegetation. In

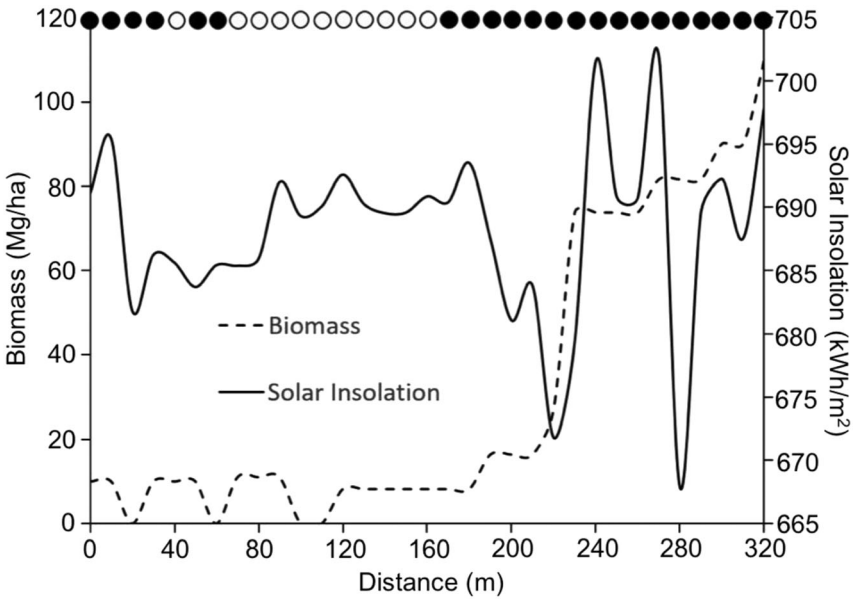

FIGURE 14 Plots of solar insolation (solid line) and biomass (dashed line) relative to areas interpreted to have permafrost or frozen layers (black circles) or no permafrost (hollow circles) along line 1 at the northwest corner of Twelvemile Lake

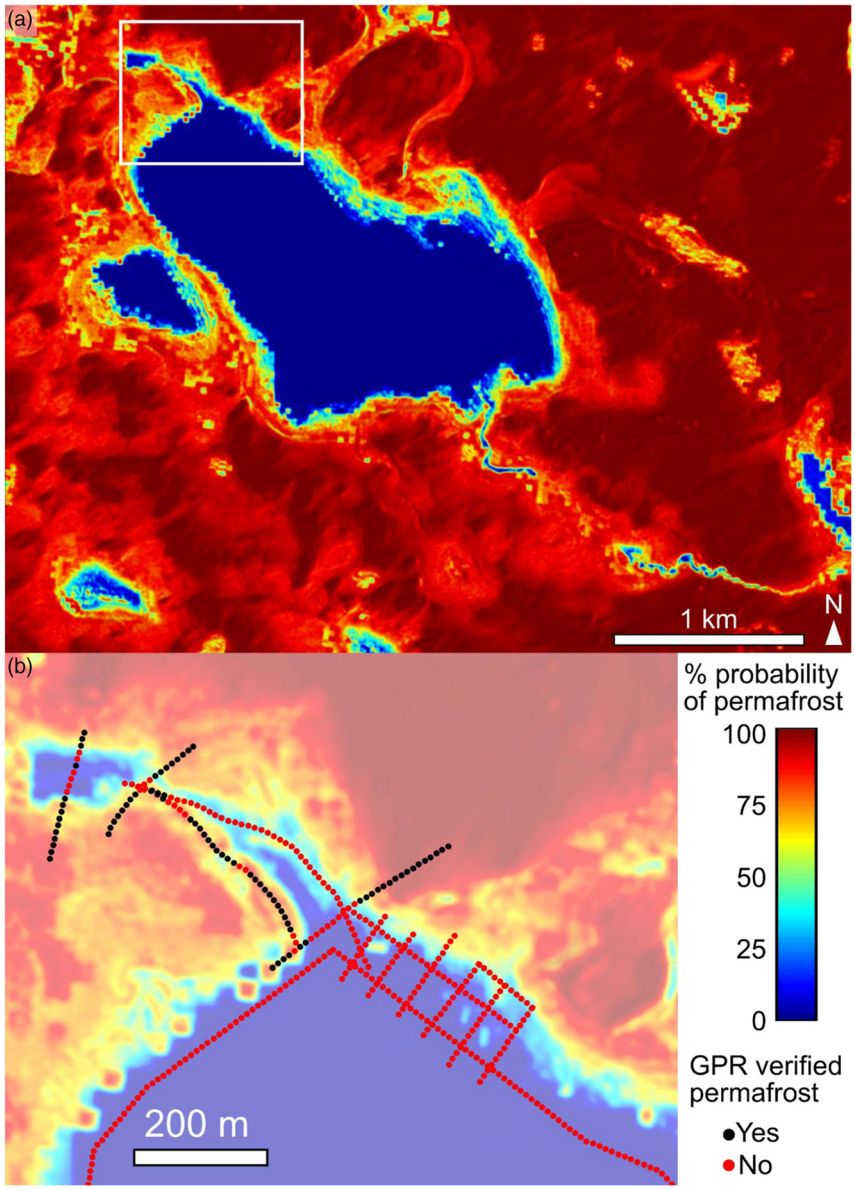

FIGURE 15 (a) ANN permafrost classification map, where colors denote probability of permafrost presence. (b) Zoom of northwest outlet with overlain GPR transects

these locations, we infer low to moderate permafrost probability as an indication of active layer presence over permafrost or near-surface frozen layers from winter that have not yet thawed during the summer. We define transitional ground-freezing as ground that freezes during the winter that may or may not thaw again during summer months. Regions where active vegetation succession trends towards greater biomass over time may eventually allow thin frozen layers to form and remain through the duration of consecutive summers, thereby forming permafrost due to increasing thermal protection. The northwest outlet of Twelvemile Lake may represent a prime example of this potential process.

To extend beyond our classification results and predict thaw depth in these complex regions we performed secondary regression analyses to identify correlative trends between ANN probabilities and FDEM data (Figure 16) collected along lines 1 and 2 of the northwest outlet. We determined two major resistivity thresholds from FDEM inversions for a series of depth increments to a maximum depth of 4 m,[83] one representing transitional ground freezing at 300 Ω.m, and a second threshold, generally identified at greater depth, representing solid permafrost at 380 Ω.m. Model results indicate relatively strong correlation between ANN-derived permafrost probability and the transitional ground freezing (R = −0.77) and solid permafrost (R = −0.74) thresholds. In general, for locations where we map less than 90% probability for the presence of permafrost, we also predict the presence of thawing at the surface. The thaw depth thickens linearly with decreasing permafrost probability. Permafrost is present at the surface for locations with permafrost probability ≥95%. The maximum measurable depth to permafrost is 4 m and co-occurs with a thaw depth of 1.2 m, predicted to occur for locations with permafrost probability of 73%. The maximum measurable thaw depth is 4 m and is predicted to occur for locations with permafrost probability of 32%. These results indicate that permafrost is effectively absent in our measurable depth range for locations with permafrost probability <73% and it is present near the surface where probability is ≥95%. Locations that exhibit occasional thawing, with thermal conditions that are intermittently similar to permafrost, occur where permafrost probability is in the range 32–90%. Locations with probability <32% are not expected to have conditions conducive to permafrost or thawing in our measurable depth range.

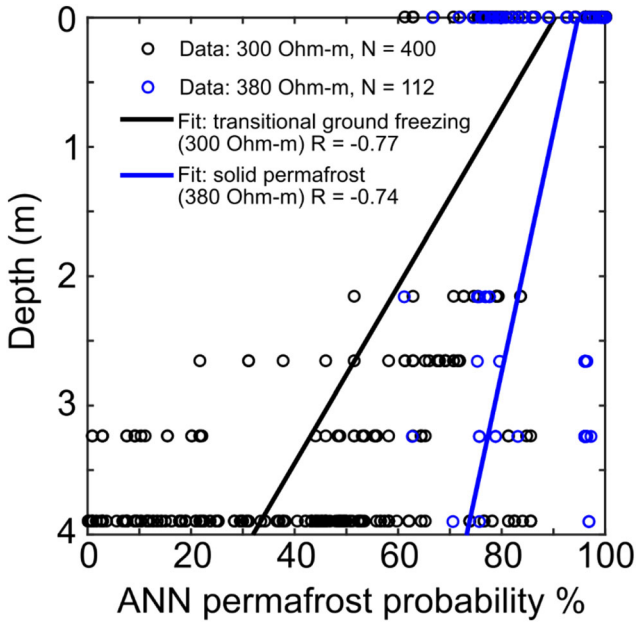

FIGURE 16 Regression plot identifying correlative trends between ANN probabilities and depth to frozen ground, derived from FDEM field analysis. Thresholds for conditions of transitional ground freezing and solid permafrost were determined from resistivity values of 300 and 380 Ω.m, respectively

5 | POTENTIAL UPSCALING ACROSS BROADER REGIONS

Results from this study show quantitative relationships between GPR and FDEM-mapped permafrost distribution to vegetation biomass and modeled solar insolation determined from DEM analysis. Observable relationships between permafrost extent and terrain or vegetation cover have been established for decades.[39,41] However, very few ground-based methods can rapidly survey large areas efficiently and effectively to map the permafrost extent under the active layer in discontinuous permafrost regions across variable terrain and vegetation cover. GPR and FDEM are two such methods that can cover relatively large distances over rough terrain to determine, in most cases, the presence or absence of frozen ground, thaw depth, or thickness of the active layer. In this case, we show that remote sensing datasets in conjunction with GPR and FDEM can be used to laterally extrapolate geophysical observations of frozen ground or permafrost. Unfortunately, field observations are rare in the Arctic due to its remoteness and rough terrain. Our data were collected on foot in August and via snow machine in April.[28] Both methods covered substantial distances, terrain, and biomass regimes over short periods of time, showing the efficacy of ground-based GPR and FDEM to rapidly estimate the presence of permafrost for comparison to remotely sensed datasets. Our results additionally show the potential value of neural network machine learning methods to spatially quantify the probability of permafrost and to estimate thaw layer thicknesses based on multiple observational inputs (GPR, FDEM, biomass cover, and modeled solar insolation). To further expand our ANN-based permafrost classification and ANN-FDEM linear regression analysis beyond the Twelvemile Lake region would require a greater number of field measurements across a broader diversity of Arctic terrain. Without additional geophysical observations in more diverse terrain, many assumptions would be required to perform a similar analysis. A combination of ArcticDEM, ICESat-2, and further Landsat analyses may provide insolation and biomass calculations across broader regions for comparison to collected geophysical data within different Arctic terrain or vegetation environments to capture permafrost complexities using multivariable analysis[87–90] or ANN methods. This said, satellite-derived bare earth accuracy may require initial in-situ ground-truth to ensure accuracy because biomass cover and associated reflectivity will impact results.

6 | CONCLUSIONS

Seasonal thaw, associated active layer thickness, and the distribution of permafrost are complex in Alaska due to natural fluvial, geomorphological, and vegetation succession processes. Other natural factors such as terrain aspect, forest fires, snow cover, and seasonal air temperatures also alter active layer, permafrost, and seasonal freeze patterns. Our results show that high-resolution DEM analysis, Landsat-derived above-ground biomass measurements, geophysical observations, and machine learning can be coupled to estimate the lateral extent of permafrost or seasonal freeze and thaw depths within the active layer. We show that biomass as low as 15 Mg/ha is enough to allow seasonal freezing to persist through August, particularly in regions receiving low solar insolation due to a north-facing terrain aspect. Likewise, biomass values of 90–140 Mg/ha are enough to protect thick permafrost on south-facing slopes. Although depth and thickness of permafrost or seasonal freeze may not solely correspond to terrain features or above-ground biomass, determining the presence or absence of frozen ground provides a starting point for targeted ground-truth studies using geophysical methods such as FDEM or GPR. Our study at Twelvemile Lake shows promise in extrapolating to larger regions of the Arctic by using more extensive satellite or airborne remote sensing platforms, selected ground-truth sites, and machine learning.

ACKNOWLEDGEMENTS

Funding for this project was provided by the Strategic Environmental Research and Development Program (awards RC-2110 and RC-2111) and the U.S. Army Corps of Engineers Research and Development Center Directed and Basic Research Programs. Polar Geospatial Center-derived DEMs were created from DigitalGlobe, Inc., imagery and were funded under National Science Foundation awards 1043681, 1559691, and 1542736. We appreciate field assistance from Emily Voytek, Fred Day-Lewis, and Doug Halm. We also appreciate support from lead project investigators Beth Astley and Michelle Walvoord. Any use of trade, firm, or product names is for descriptive purposes only and does not imply endorsement by the U.S. Government. The data that support the findings of this study are available as detailed in the main reference list,[86] and from the corresponding author upon reasonable request.

ORCID

Seth William Campbell https://orcid.org/0000-0002-9620-8329
Martin Briggs https://orcid.org/0000-0003-3206-4132
Samuel G. Roy https://orcid.org/0000-0002-2491-948X
Thomas A. Douglas https://orcid.org/0000-0003-1314-1905

REFERENCES

1. Zhang T, Barry RG, Knowles K, Heginbottom JA, Brown J. Statistics and characteristics of permafrost and ground-ice distribution in the northern hemisphere. *Polar Geogr*. 1999;23(2):132-154.
2. Brown J, Haggerty C. Permafrost digital databases now available. *EOS (Trans Amer Geophys Union)*. 1998;79(52):634.
3. Jorgenson MT, Racine CH, Walters JC, Osterkamp TE. Permafrost degradation and ecological changes associated with a warming climate in Central Alaska. *Clim Change*. 2001;48(4):551-579.
4. Brown J, Ferrians OJ, Heginbottom JA, Melnikov ES. *Circum-Arctic map of permafrost and ground ice conditions. V2*. Boulder, CO: National Snow and Ice Data Center; 2002.
5. Osterkamp TE, Romanovsky VE. Evidence for warming and thawing of discontinuous permafrost in Alaska. *Permafr Periglac Process*. 1999;10(1):17-37.
6. Douglas TA, Jones MC, Hiemstra CA, Arnold J. Sources and sinks of carbon in boreal ecosystems of interior Alaska: current and future perspectives for land managers. *Elementa: Sci Anthro*. 2014;1-39. https://doi.org/10.12952/journal.elementa.000032#sthash.j8pzVjml.dpuf
7. Loranty MM, Abbott BW, Blok D, et al. Reviews and syntheses: changing ecosystem influences on soil thermal regimes in northern high-latitude permafrost regions. *Biogeosciences*. 2018 Aug 31;15(17):5287-5313.
8. Shur YL, Jorgenson MT. Patterns of permafrost formation and degradation in relation to climate and ecosystems. *Permafr Periglac Process*. 2007;18(1):7-19. https://doi.org/10.1002/ppp.582, 18, 1, 7, 19.
9. Nelson FE, Shiklomanov NI, Mueller GR, Hinkel KM, Walker DA, Bockheim JG. Estimating active-layer thickness over a large region: Kuparuk River basin, Alaska, U.S.A. *Arctic Alpine Res*. 1997;29(4):367-378.
10. Nelson FE, Hinkel KM, Shiklomanov NI, Mueller GR, Miller LL, Walker DA. Active-layer thickness in north Central Alaska: systematic sampling, scale, and spatial autocorrelation. *J Geophys Res*. 1998;103(D22):28,963-28,973.
11. Liu L, Schaefer K, Zhang T, Wahr J. Estimating 1992–2000 average active layer thickness on the Alaskan north slope from remotely sensed surface subsidence. *J Geophys Res*. 2012;117(F01005):1-14. https://doi.org/10.1029/2011JF002041
12. Mishra U, Riley WJ. Active-layer thickness across Alaska: comparing observation-based estimates with CMIP5 earth system model predictions. *Soil Soc Am J*. 2014;78(3):894-902. https://doi.org/10.2136/sssaj2013.11.0484
13. Widhalm B, Bartsch A, Leibman M, Khomutov A. Active-layer thickness estimation from X-band SAR backscatter intensity. *The Cryosph*. 2017;11(1):483-496. https://doi.org/10.5194/tc-11-483-2017
14. Douglas TA, Jorgenson MT, Kanevskiy MZ, Romanovsky VR, Shur Y, Yoshikawa K. Investigations into permafrost dynamics at the Fairbanks permafrost Experimental Station near Fairbanks, Alaska. *Proc Ninth Intern Conf Permaf*. 2008;373-378.
15. Douglas TA, Jorgenson MT, Brown DRN, et al. Degrading permafrost mapped with electrical resistivity tomography, airborne imagery and LiDAR, and seasonal thaw measurements. *Geophysics*. 2016;81(1):WA71-WA85. https://doi.org/10.1190/GEO2015-0149.1
16. Romanovsky VE, Smith SL, Isaksen K, et al. Terrestrial permafrost [in Arctic Report Card 2017]; 2017. http://www.arctic.noaa.gov/Report-Card
17. Schuur EAG, Vogel JG, Crummer KG, Lee H, Sickman JO, Osterkamp. The effect of permafrost thaw on old carbon release and net carbon exchange from tundra. *Nature*. 2009;459(7246):556-559.
18. Deconto RM, Galeotti S, Pagani M, et al. Past extreme warming events linked to massive carbon release from thawing permafrost. *Nature*. 2012;484(7392):87-91.
19. Tarnocai C, Canadell JG, Schuur EAG, Kuhry P, Mazhitova G, Zimov S. Soil organic carbon pools in the northern circumpolar permafrost region. *Global Biogeochem Cy*. 2009;23(2):GB2023. https://doi.org/10.1029/2008GB003327
20. Hugelius G, Strauss J, Zubrzycki S, et al. Estimated stocks of circumpolar permafrost carbon with quantified uncertainty ranges and

identified data gaps. *Biogeosciences*. 2014;11(23):6573-6593. https://doi.org/10.5194/bg-11-6573-2014
21. Verpaelst M, Fortier D, Kanevskiy M, Paquette M, Shur Y. Syngenetic dynamic of permafrost of a polar desert solifluction lobe, Ward Hunt Island, Nunavut. *Arctic Sci*. 2017;3:301-319. https://doi.org/10.1139/as-2016-0018
22. Kokelj SV, Lacelle D, Lantz TC, et al. Thawing of massive ground ice in mega slumps drives increases in stream sediment and solute flux across a range of watershed scales. *J Geophys Res*. 2013;118(2):681-692. https://doi.org/10.1002/jgrf.20063
23. Ponti S, Cannone N, Guglielmin M. A new simple topo-climatic model to predict surface displacement in paraglacial and periglacial mountains of the European Alps: the importance of ground heating index and floristic components as ecological indicators. *Ecol Indic*. 2021;120(106889):1–10.
24. Melvin AM, Larsen P, Boehlert B, et al. Climate change damages to Alaska public infrastructure and the economics of proactive adaptation. *Proc Natl Acad Sci*. 2016;114(2):E122-E131. https://doi.org/10.1073/pnas.1611056113
25. Jepsen SM, Walvoord MA, Voss CI, Rover JR. Effect of permafrost thaw on the dynamics of lakes recharged by ice-jam floods: case study of Yukon flats, Alaska. *Hydrol Process*. 2016;30:1782-1795. https://doi.org/10.1002/hyp.10756
26. Jepsen SM, Voss CI, Walvoord MA, Rose JR, Minsley BJ, Smith BD. Sensitivity analysis of Lake mass balance in discontinuous permafrost: the example of disappearing twelve-mile lake, Yukon flats, Alaska (USA). *Hydrgeol J*. 2013a;21(1):185-200. https://doi.org/10.1007/s10040-012-0896-5
27. Briggs MA, Walvoord MA, McKenzie JM, Voss CI, Day-Lewis FD, Lane JW. New permafrost is forming around shrinking Arctic lakes, but will it last? *Geophys Res Lett*. 2014;41(5):1585-1592. https://doi.org/10.1002/2014GL059251
28. Briggs M, Campbell S, Nolan J, Ntarlagiannis D, Day-Lewis F, Lane J. Geophysical methods for characterizing the active layer and new permafrost formation. *Permafr Perigl Proc*, 15 pp. 2017;28(1):52-65. https://doi.org/10.1002/ppp.1893
29. Ling F, Tingiun Z. Modeled impacts of changes in tundra snow thickness on ground thermal regime and heat flow to the atmosphere in northernmost Alaska. *Global Planet Change*. 2007;57(3-4):235-246.
30. Ling F, Zhang T. Impact of the timing and duration of seasonal snow cover on the active layer and permafrost in the Alaskan Arctic. *Permafrost Peri Proc*. 2003;14(2):141-150. https://doi.org/10.1002/ppp.445
31. Johansson M, Callaghan TV, Bosiö J, Åkerman HJ, Jackowicz-Korczynski M, Christensen TR. Rapid responses of permafrost and vegetation to experimentally increased snow cover in sub-arctic Sweden. *Environ Res Lett*. 2013;8(3):1–10.
32. Liston G, Sturm M. A snow-transport model for complex terrain. *J Glaciol*. 1998;44(148):498-516.
33. Nguyen TN, Burn CR, King DJ, Smith SL. Estimating the extent of near surface permafrost using remote sensing, Mackenzie Delta, Northwest Territories. *Perma Perig Proc*. 2009;20(2):141-153.
34. Panda SK, Prakash A, Solie DN, Romanovsky VE, Jorgenson MT. Remote sensing and field-based mapping of permafrost distribution along the Alaska highway corridor, interior Alaska. *Perma Perig Proc*. 2010;21(3):271-281.
35. Jorgenson T, Yoshikawa K, Kanevskiy M, et al. *Map of Permafrost Characteristics of Alaska*. Institute of Northern Engineering, University of Alaska, Fairbanks; 2008. http://permafrost.gi.alaska.edu/sites/default/files/AlaskaPermafrostMap_Front_Dec2008_Jorgenson_etal_2008.pdf
36. Minsley BJ, Abraham JD, Smith BD, et al. Airborne electromagnetic imaging of discontinuous permafrost. *Geophys Res Lett*. 2012;39(2):1-8. https://doi.org/10.1029/2011GL050079
37. Parsekian AD, Grosse G, Walbrecker JO, et al. Detecting unfrozen sediments below thermokarst lakes with surface nuclear magnetic resonance. *Geophys Res Lett*. 2013;40(3):535-540. https://doi.org/10.1002/grl.50137
38. Walter KM, Smith LC, Chapin FS. Methane bubbling from northern lakes: present and future contributions to the global methane budget. *Philos Trans R Soc, Ser A*. 2007;365(1856):1657-1676. https://doi.org/10.1098/rsta.2007.2036
39. Peddle DR, Franklin SE. Multisource evidential classification of surface cover and frozen ground. *Intern J Re Sen*. 1992;13(17):3375-3380.
40. Leverington DW, Duguay CR. A neural network method to determine the presence or absence of permafrost near Mayo, Yukon territory, Canada. *Perma Perig Proc*. 1997;8:207-217.
41. Peddle DR, Franklin SE. Classification of permafrost active layer depth from remotely sensing and topographic evidence. *Remote Sens Envir*. 1993;44(1):67-80.
42. Leverington DW, Duguay CR. Evaluation of three supervised classifiers in mapping depth to late-summer frozen ground, Central Yukon territory. *Canadian J Re Sen*. 1996;22(2):163-174.
43. Chasmer L, Quinton W, Hopkinson C, Petrone R, Whittington P. Vegetation canopy and radiation controls on permafrost plateau evolution within the discontinuous permafrost zone, Northwest Territories, Canada. *Perma Perig Proc*. 2011;22:199-213.
44. Pastick NJ, Jorgenson MT, Wylie BK, Rose JR, Rigge M, Walvoord MA. Spatial variability and landscape controls of near-surface permafrost within the Alaskan Yukon River basin. *J Geophys Res Biogeosci*. 2014;119(6):1244-1265. https://doi.org/10.1002/2013JG002594
45. Anderson JE, Douglas TA, Barbato RA, Saari S, Edwards JD, Jones RM. Linking vegetation cover and seasonal thaw depths in interior Alaska permafrost terrains using remote sensing. *Remote Sens Environ*. 2019 Nov 1;233:111363.
46. Brown DRN, Jorgenson MT, Douglas TA, Romanovsky V, Kielland K, Euskirchen E. Vulnerability of permafrost to fire-initiated thaw in lowland forests of the Tanana flats, interior Alaska. *J Geop Res Biogeosci*, 19 pages. 2015;120(8):1619-1637. https://doi.org/10.1002/2015JG003033
47. Hrbáček F, Cannone N, Kňažková M, Malfasi F, Convey P, Guglielmin M. Effect of climate and moss vegetation on ground surface temperature and the active layer among different biogeographical regions in Antarctica. *Catena*. 2020;190(104562).
48. Lin L, Zhang T, Wahr J. InSAR measurements of surface deformation over permafrost on the north slope of Alaska. *J Geophys Res*. 2010;115(F3):1-14, F03023. https://doi.org/10.1029/2009JF001547
49. Shiklomanov NI, Streletskiy DA, Little JD, Nelson FE. Isotropic thaw subsidence in undisturbed permafrost landscapes. *Geophys Res Lett*. 2013;40(24):6356-6361. https://doi.org/10.1002/2013GL058295
50. Wellman TP, Voss CI, Walvoord MA. Impacts of climate, lake size, and supra and sub-permafrost groundwater flow on lake-talik evolution, Yukon flats, Alaska (USA). *Hydrgeol J*. 2013;21(1):281-298. https://doi.org/10.1007/s10040-012-0941-4
51. Jepsen SM, Koch JC, Rose JR, Voss CI, Walvoord MA. Thermal and hydrological observations near Twelvemile Lake in discontinuous permafrost, Yukon flats, interior Alaska, September 2010-august 2011. *USGS Open-File Rep*. 2012;25:2012-1121.
52. Jepsen SM, Voss CI, Walvoord MA, Minsley BJ, Rover J. Linkages between lake shrinkage/expansion and sublacustrine permafrost distribution determined from remote sensing of interior Alaska,USA. *Geophy Res Lett*. 2013b;40(5):882-887. https://doi.org/10.1002/grl.50187
53. Hoekstra P. Electromagnetic methods for mapping shallow permafrost. *Geophysics*. 1978;43(4):782-787.

54. Minsley BJ, Wellman TP, Walvoord MA, Revil A. Sensitivity of airborne geophysical data to sublacustrine and near-surface permafrost thaw. *The Cryosph*. 2015;9(2):781-794.
55. Briggs, M.A., Nelson, N, Gardner, P, Solomon, K., Terry, N., and Lane, J.W., 2019, Wetland-scale mapping of preferential fresh groundwater discharge to the Colorado River, groundwater, https://doi.org/10.1111/gwat.12866
56. Sheets RA, Dumouchelle DH. *Geophysical investigation along the great Miami River from new Miami to Charles M. Bolton Well Field, Cincinnati, Ohio. U.S. Geol. Surv. Open File Rep 2009–1025*. Reston, VA: USGS; 2009.
57. Ong JB, Lane JW, Zlotnik VA, Halihan T, White EA. Combined use of frequency-domain electromagnetic and electrical resistivity surveys to delineate near-Lake groundwater flow in the semi-arid Nebraska Sand Hills, USA. *Hydrogeol J*. 2010;18(6):1539-1545.https://doi.org/10.1007/s10040-010-0617-x
58. Ji L, Wylie BK, Nossov DR, et al. Estimating aboveground biomass in interior Alaska with Landsat data and field measurements. *Intern J Applied Earth Observ Geoinf*. 2012;18:451-461.
59. Rich PM, Dubayah R, Hetrick WA, Saving SC. Using Viewshed models to calculate intercepted solar radiation: applications in ecology. *Amer Soc Photogram Remote Sens Tech Pap*. 1994;524-529.
60. Fu P, Rich PM. *The solar analyst 1.0 manual*. USA: Helios environmental modeling institute (HEMI); 2000.
61. Fu P, Rich PM. A geometric solar radiation model with applications in agriculture and forestry. *Compu Electro Agricu*. 2002;37(1-3):25-35.
62. USGS Earth Resources Observation and Science (EROS) Center. 2012. Aboveground Biomass in Yukon Flats Ecoregion, Version 2. https://lca.usgs.gov/lca/yukonflats_biomass/index.php
63. Pastick NJ, Jorgenson MT, Wylie BK, et al. Extending airborne electromagnetic surveys for regional active layer and permafrost mapping with remote sensing and ancillary data, Yukon flats ecoregion, Central Alaska. *Permafr Periglac Process*. 2013;24(3):184-199. https://doi.org/10.1002/ppp.1775
64. Ulrich M, Hauber E, Herzschuh U, Härtel S, Schirrmeister L. Polygon pattern geomorphometry on Svalbard (Norway) and western utopia Planitia (Mars) using high-resolution stereo remote-sensing data. *Geomorphology*. 2011;134(3-4):197-216. https://doi.org/10.1016/j.geomorph.2011.07.002
65. Haltigin TW, Pollard WH, Dutilleul P, Osinski GR. Geometric evolution of polygonal terrain networks in the Canadian high Arctic: evidence of increasing regularity over time. *Perma Perig Proc*. 2012;23(3):178-186. https://doi.org/10.1002/ppp.1741
66. Skurikhin AN, Gangodagamage C, Rowland JC, Wilson CJ. Arctic tundra ice-wedge landscape characterization by active contours without edges and structural analysis using high-resolution satellite imagery. *Remote Sen Lett*. 2013;4(11):1077-1086. https://doi.org/10.1080/2150704X.2013.840404
67. Skurikhin AN, Wilson CJ, Liljedahl A, Rowland JC. Recursive active contours for hierarchical segmentation of wetlands in high-resolution satellite imagery of Arctic landscapes. *2014 South Sympo Image Analy Interpret*. 2014;137-140. https://doi.org/10.1109/SSIAI.2014.6806048
68. Gangodagamage C, Rowland JC, Hubbard SS, et al. Extrapolating active layer thickness measurements across Arctic polygonal terrain using LiDAR and NDVI data sets: research article. *Water Resour Res*. 2014;50(8):6339-6357. https://doi.org/10.1002/2013WR014283
69. Wainwright HM, Dafflon B, Smith LJ, et al. Identifying multiscale zonation and assessing the relative importance of polygon geomorphology on carbon fluxes in an Arctic tundra ecosystem. *J Geophys Res Biogeo*. 2015;120(4):788-808. https://doi.org/10.1002/2014JG002799
70. Steedman AE, Lantz TC, Kokelj SV. Spatio-temporal variation in high-Centre polygons and ice-wedge melt ponds, Tuktoyaktuk coastlands, Northwest Territories: variation in high-Centre polygons and ice-wedge melt ponds. *Permafro Peri pro*. 2017;28(1):66-78. https://doi.org/10.1002/ppp.1880
71. Perreault N, Lévesque E, Fortier D, Gratton D, Lamarque LJ. Remote sensing evaluation of high Arctic wetland depletion following permafrost disturbance by thermo-erosion gullying processes. *Arctic Sci*. 2017;3(2):237-253. https://doi.org/10.1139/as-2016-0047
72. Chen Z, Pasher J, Duffe J, Behnamian A. Mapping Arctic coastal ecosystems with high resolution optical satellite imagery using a hybrid classification approach. *Canadian J Re Sen*. 2017;43(6):513-527. https://doi.org/10.1080/07038992.2017.1370367
73. Zhang W, Witharana C, Liljedahl A, Kanevskiy M. Deep convolutional neural networks for automated characterization of Arctic ice-wedge polygons in very high spatial resolution aerial imagery. *Remote Sens (Basel)*. 2018;10(1487):1-31. https://doi.org/10.3390/rs10091487
74. Nitze I, Grosse G, Jones BM, et al. Landsat-based trend analysis of lake dynamics across northern permafrost regions. *Remote Sens (Basel)*. 2017;9(7):1-28. https://doi.org/10.3390/rs9070640
75. Ulrich M, Grosse G, Strauss J, Schirrmeister L. Quantifying wedge-ice volumes in Yedoma and Thermokarst Basin deposits. *Permafr Perig Proc*. 2014;25(3):151-161. https://doi.org/10.1002/ppp.1810
76. Barnhart KR, Anderson RS, Overeem I, Wobus C, Clow GD, Urban FE. Modeling erosion of ice-rich permafrost bluffs along the Alaskan Beaufort Sea coast. *J Geophys Res Earth*. 2014;119(5):1155-1179. https://doi.org/10.1002/2013JF002845
77. Novikova A, Belova N, Baranskaya A, et al. Dynamics of permafrost coasts of Baydaratskaya Bay (Kara Sea) based on multi-temporal remote sensing data. *Remote Sens (Basel)*. 2018;10(9):1-30. https://doi.org/10.3390/rs10091481
78. Kohavi R. A study of cross-validation and bootstrap for accuracy estimation and model selection. *Intern Joint Conf Artifi Intel*. 1995;14(2):1137-1145.
79. Arcone SA, Delaney AJ. Field dielectric measurements of frozen silt using VHF pulses. *Cold Reg Sci Technol*. 1984;9(1):29-37.
80. Arcone SA, Lawson DE, Delaney AJ. Short-pulse radar wavelet recovery and resolution of dielectric contrasts within englacial and basal ice of Matanuska glacier, Alaska, U.S.A. *J Glaciol*. 1995;44(137):68-86.
81. Lawson DE, Strasser JC, Strasser JD, Arcone SA, Delaney AJ, Williams C. Geological and geophysical investigations of the hydrogeology of fort Wainwright, Alaska part 1: Canol road area. *CRREL Report*. 1996;94, 31 pp-96.
82. Arcone SA, Lawson DE, Delaney AJ, Strasser JC, Strasser JD. Ground-penetrating radar reflection profiling of groundwater and bedrock in an area of discontinuous permafrost. *Geophysics*. 1998;63(5):1573-1584.
83. Lawson DE, Arcone SA, Delaney AJ, Strasser JD, Strasser JC, Hall TJ. Geological and geophysical investigations of the hydrogeology of Fort Wainwright. Alaska Part II: North-Central Cantonment Area. CRREL Report; 1998:98-96 72 pp.
84. Wooldridge CL, Hickin EJ. Radar architecture and evolution of channel bars in wandering gravel-bed rivers: Fraser and Squamish Rivers, British Columbia, Canada. *J Sed Rese*. 2005;2005, 75:844-860. https://doi.org/10.2110/jsr.2005.066
85. Bridge JS, Lunt IA. In: Smith GHS, Best JL, Bristow CS, Petts GE, eds. *Depositional models of braided Rivers, in braided Rivers: process, deposits, ecology and management*. Oxford, UK: Blackwell publishing ltd; 2006 10.1002/9781444304374.ch2.
86. Briggs MA, White EA, Lane JW. *Surface geophysical data for characterizing shallow, discontinuous frozen ground near Fort Yukon*. Alaska: U.S.

Geological Survey data release; 2020. https://doi.org/10.5066/P9UST855
87. Jones BM, Stoker JM, Gibbs AE, et al. Quantifying landscape change in an arctic coastal lowland using repeat airborne LiDAR. *Environ Res Lett*. 2013;8(4):1-10, 045025. https://doi.org/10.1088/1748-9326/8/4/045025
88. Moussavi MS, Abdalati W, Scambos T, Neuenschwander A. Applicability of an automatic surface detection approach to micropulse photon-counting lidar altimetry data: implications for canopy height retrieval from future ICESat-2 data. *Intern J Re Sen*. 2014;35(13):5263-5279. https://doi.org/10.1080/01431161.2014.939780
89. Brown ME, Arias SD, Neumann T, et al. Applications for ICESat-2 data. *IEEE Geoscience and Remote Sensing*December. 2016;24-37. https://doi.org/10.1109/MGRS.2016.2560759
90. Narine LL, Popescu SC, Malambo L. Using ICESat-2 to estimate and map Forest aboveground biomass: a first example. *Remote Sens (Basel)*. 2020;12(1824):1-16.

How to cite this article: Campbell SW, Briggs M, Roy SG, Douglas TA, Saari S. Ground-penetrating radar, electromagnetic induction, terrain, and vegetation observations coupled with machine learning to map permafrost distribution at Twelvemile Lake, Alaska. *Permafrost and Periglac Process*. 2021;1–20. https://doi.org/10.1002/ppp.2100